RHEOLOGICAL AND THERMAL CHARACTERIZATION OF 3D PRINTABLE LIGHTWEIGHT CEMENTITIOUS COMPOSITES WITH FLY ASH CENOSHPERES

A Thesis

By

Yang Yang

Submitted to School of Engineering and Applied Science of

University of Virginia

In partial fulfillment of the requirements of the degree of

MASTER OF SCIENCE

In

Civil Engineering

July 2021

ABSTRACT

The thermally poor design of residential and commercial buildings considerably increases heating and cooling demands which lead to an increase in energy consumption and carbon emissions. Recent advances in cement-based composites offer improved thermal properties and lower embodied energy and emission using functional fillers and supplemental cementitious materials. 3D printing of cement-based composites also allows structural members to be produced in complex shapes that are not possible to achieve with traditional methods. In 3D printed concrete structures, the inner and outer geometries of building walls can be optimized to receive, store and dissipate thermal energy depending on the needs of the building's climate. Combining advantages offered by advanced materials and digital fabrication can improve energy use during the construction phase as well as the life cycle of a building.

Towards this goal, this thesis investigates the development of fly ash cenoshperes (FAC) based lightweight cementitious composites that can be used as both structural and nonstructural material in digital construction. FACs are hollow alumino-silicate spheric particles obtained as a by-product of a thermal power plant's coal combustion. The hollow and air-filled nature of FACs can lead to a considerable reduction in thermal conductivity and density of cementitious composites. Portland cement, fine sand, silica fume, water, FACs, water reducer and viscosity modifying agent (VMA) are used to fabricate 3D printable lightweight cementitious composites. The effect of FACs to sand volume ratio and VMA to binder ratio on rheological, mechanical and thermal properties of developed composites are studied. Rheological tests are conducted using a shear rheometer. Yield stress and apparent viscosity of the FACs-based cement mixtures with four different FACs to sand volume ratios and four different VMA to binder ratios are determined by stress growth tests. Cubic specimens are prepared to determine the compressive

strength of the developed composites. A heat flow meter technique is employed to determine the thermal conductivity of the developed composites with different FACs volume ratios. Prismatic specimens are cast and cured for 28 days for thermal tests. Printability of the most promising mixture proportion is assessed using a 3D concrete printer equipped with a screw pump and two different nozzles. Results show that thermal conductivity is inversely correlated with FACs content. By replacing 60% of sand with FACs and using VMA at 0.3% by weight of binder in a mortar composite, a printable lightweight cementitious composite with good thermal and mechanical properties can be obtained.

DEDICATION

I would like to dedicate this thesis to my parents, Huigeng Yang and Qun Shi for their endless support.

ACKNOWLEDGMENTS

I would like to thank the faculty and staff of the Department of Engineering Systems and Environment of University of Virginia. In particular, I would like to express my most sincere gratitude to my advisor, Dr. Osman Ozbulut, for his guidance and support for my thesis work. In addition, I would like to thank Dr. Jose Gomez and Dr. Ji Ma for serving on my thesis defense committee.

I would like to thank Dr. Richard White for his technical support on the SEM test. I would also like to thank Dr. Derek Henderson for his assistance on laboratory equipment usage. In addition, I would like to express my appreciation to my laboratory mates, Ugur Kilic and Zhangfan Jiang for their assistance on my research.

NOMENCLATURE

FAC	Fly-Ash Cenoshpere
VMA	Viscosity Modifying Agent
SF	Silica Fume
EA	Expansive Agent
WR	Water Reducer
HFM	Heat Flow Meter

TABLE OF CONTENTS

LIST OF TABLES

LIST OF FIGURES

1. INTRODUCTION

1.1. Motivation

As the negative effects of climate change is becoming more and more evident in today's world, civil engineers are facing a challenging task: improving efficiency and reducing environmental impacts of construction industry. One challenge is energy-efficiency in residential and commercial buildings. Thermally poor design of residential buildings considerably increases heating and cooling demands that lead to an increase in energy consumption and carbon emissions [1,2]. For cold regions where heating loads dominate energy consumption, low thermal transmittance of building envelope, especially walls, and air leakage are the most critical parameters in achieving energy efficiency in residential buildings [3].

Indeed, heating and cooling inside a building is the major source of energy consumptions in daily operation of the building. Based on the data released from U.S. Energy Information Administration, in 2015, the main energy consumption for variety types of homes is due to spacing heating [4]. For most of types of U.S homes, space heating and air conditioning take up to half or more than half of the entire energy consumption of households. Reducing the thermal conductivity of the walls and structural members of a building can be feasible way to improve the efficiency of the building. The buildings constructed with such materials will require considerably less heating and cooling to maintain a constant temperature inside.

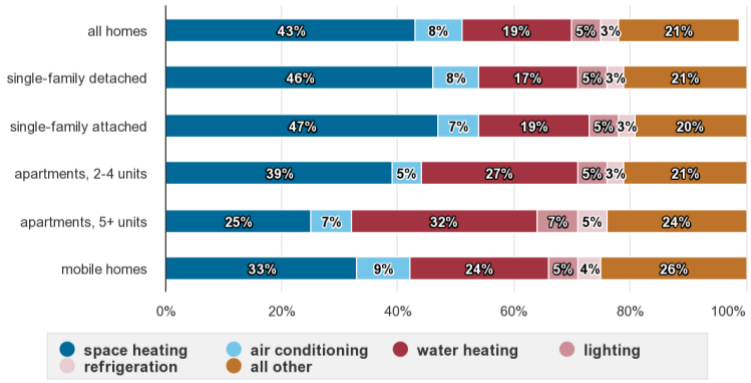

Figure 1. End-use consumption shares by types of U.S homes, 2015 [4]

Recent advances in cement-based composites offer improved thermal properties and lower embodied energy and emission through the use of functional fillers, supplemental cementitious materials, or natural fibers. Lightweight concrete possesses advantageous such as lower thermal conductivity and higher fire resistance over normal weight concrete. Lightweight cementitious composites can reduce the self-weight of the structural members, which can lead to smaller members sizes and foundation size [5].

Traditionally, lightweight aggregates such as expanded perlite and shale or air-entraining agents are added to the mixture develop lightweight concrete [6,7]. More recently, lightweight fillers such as expanded polysterene beads, hollow glass microspheres, and fly ash cenospheres (FACs) are also used for the development of lightweight cementitious composites [8]. FACs are hollow alumino-silicate particles obtained as a by-product of thermal power plant's coal combustion. The air-filled core of the FACs can lead to considerable reduction in thermal conductivity and density of cementitious composites.

3D concrete printing is another novel and emerging technology in construction industry. Comparing to traditional concrete casting, 3D concrete printing avoids the need of formwork to mold concrete into the desired shape [9]. In addition, a 3D concrete printer can

construct an entire structure with the supervision of a few operators. Thus, 3D concrete printing is considered to be a more efficient and cost-effective construction method compared to traditional concrete construction. Furthermore, the reduction in formwork usage and labor decreases the environmental impact of the structure during its construction phase.

3D concrete printing also allows structural member to be produced in complex shapes that are not possible to achieve with traditional methods [10]. The inner and outer geometries of building walls can be optimized (see Figure 2) to receive, store and dissipate thermal energy depending on the needs of building's climate.

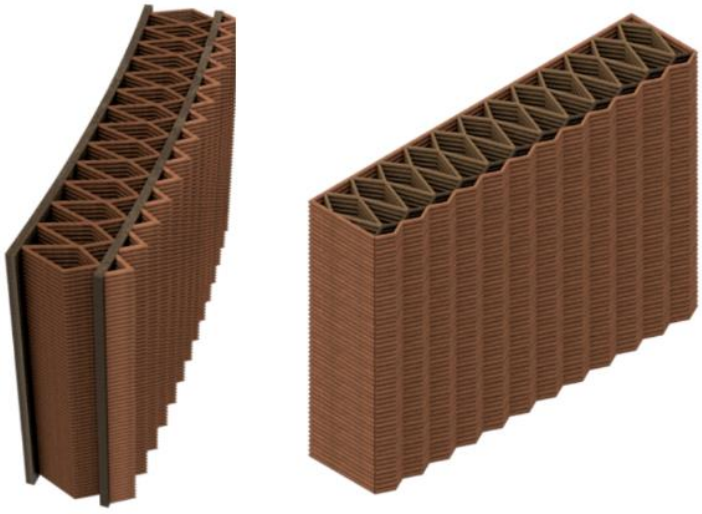

Figure 2. Design of a building wall with thermally efficient materials and infills to optimize energy efficiency.

To date, there have been several studies on the use fly ash cenoshpere to develop lightweight concrete and a large number of studies on the development of 3D printable cement composites. However, there is need for further research for exploring the use of the FACs in the development of printable cementitious material to improve thermal efficiency of 3D printed structures. Such a solution addresses both improving energy use during the construction phase as well as the life cycle phase.

1.2 Objective

In this thesis, the development of a 3D printable FACs-based lightweight cementitious composite material that can be used for both structural and non-structural used was explored. Frist, the rheological properties of FACs-based cementitious composites were studied considering the effect of FACs percentage in the mixture as well as the use of a viscosity modifying agent. A total of sixteen different mixtures were prepared for the rheological tests based on factorial design of experiments. A heat flow meter was used to determine thermal conductivity of the developed mixtures. The compressive strength of the same mixtures was also assessed. Finally, the printability of the most promising mixture was explored through direct printing tests using a 3D concrete printer with two different nozzles.

1.3 Thesis Organization

This thesis is organized into the following sections:

Chapter 1 gives a brief description of this thesis. In addition, the motivation for the research is described.

Chapter 2 presents a literature review on fly-ash cenoshperes-based cement composites and 3D printable lightweight concrete materials. It also provides some background information on thermal conductivity measurement methods.

Chapter 3 explains the material and equipment used in this research. This chapter also provides a description of mixing procedure for fabricating specimens used in experimental tests, including rheological, thermal, and compressive tests.

Chapter 4 discusses the experimental test results. This chapter also provides a discussion of the effects of VMA and FACs content on the printability and thermal conductivity of the developed composites.

Chapter 5 summarizes the findings of this study and provides recommendation for potential further research.

2. LITERATURE REVIEW AND BACKGROUND

2.1 Fly-Ash Cenoshperes-based cement composites

Fly ash cenospheres (FACs) are thin-walled and spherical alumina-silicate particles with a particle size typically ranging from 10-450 μm and density ranging from 600 to 900 kg/m^3. The air-filled core of FACs can lead to considerable reduction in thermal conductivity and density of cementitious composites. Therefore, several researchers have explored their use in cement-based composites.

Huang et al. [11] conducted a study to develop green lightweight engineered cementitious composites with high volume of industrial wastes. Fly Ash (FA) and fly ash cenoshperes (FAC) were selected to be lightweight aggregates for this lightweight composites. Iron ore taillings (IOTs) replaced sand in traditional normal weight concrete and was used as fine aggregates. Fly ash cenoshperes were used to replace volume of IOTs at two level: 60% and 100%. Two levels of fly ash to cement ratio of 2.2 and 4.4 were set to target different level of material strength. Total of six mixes were prepared to conduct tests on compressive strength, tensile strength and thermal conductivity. All the specimen for testing were cured under wet cloth in a plastic bag at room temperature until the age of 28 days. Results show that, with the replacement of IOTs completely by FAC, the density of the specimens reduced by about 15%. In addition, all specimens with some or all IOTs replaced by FAC have a density lower than 1850 kg/m^3 to be qualify as lightweight concrete. Tensile strength test results show that, when IOTs replaced by fly ash cenoshperes, tensile strength of mixture with FA/C ratio of 2.2 is higher than that of mixture with FA/C ratio of 4.4. However, the tensile strain capacity of mixture with FA/C ratio of 4.4 is larger than that of mixture with FA/C ratio of 2.2. Research reckon that increase in tensile strain capacity of mixture with FA/cement ratio of 4.4 from those with FA/cement ratio of

2.2 is due to the higher fly ash content leads to an increase in frictional bond at the interface between PVA fiber and cement matrix. Tensile strength reduces with the increase of FAC content. SEM analysis indicates that, when irregularly shaped IOTs replaced by the spherical FAC, tortuosity of fracture path along the interface was reduced, resulting a lower strength. Researchers concluded that FAC content has little influence on tensile strength, since tensile strength is determined by the properties of fiber and fiber/matrix interface. Compressive strength results ranging from 48.1 MPa to 25.0 MPa shows that all the developed lightweight cementitious composite meet the requirement of 17.5 MPa for structural lightweight concrete. Compressive strength decreased considerably from mixture with FA/cement ratio of 2.2 to mixture with FA/cement ratio of 4.4. Increase of FAC content gradually reduce the compressive strength of composites. Comparing the results for the mixtures with two FA/cement ratio of 2.2 and 4.4, thermal conductivity almost remained the same. On the other hand, there was a decrease in thermal conductivity with FAC content. Reduction in thermal conductivity was proportional to the increase in FAC content. The hollow structure of fly ash cenoshperes entraps air inside which leads to reduction in thermal conductivity of the lightweight concrete.

In another study, Zhou and Brook [12] investigated the thermal and mechanical properties of structural lightweight concrete that utilizes lightweight aggregates and fly-ash cenoshperes. Fly ash cenoshperes and fine and coarse lightweight aggregates were used to replace either or both natural fine and coarse lightweight aggregates. Steel fiber was also utilized to enhance the strength of the lightweight concrete. The water cement ratio was selected at 0.35 for normal strength mixtures and 0.27 for high strength mixtures. Several specimen groups were prepared with variation in amount of FAC and lightweight aggregates. Their results show that the high strength mixture with steel fiber reinforcement has the highest compressive strength.

However, the reduction in strength of high strength mixture with steel fiber with respect to density was also the greatest when normal weight aggregates replaced by light weight aggregates. Compressive strength of normal strength mixtures decreased less dramatically when normal weight aggregates replaced with light weight aggregates. Researchers believe that brittle nature of high strength matrix can be attributed to this phenomenon. Introduction of light weight material promoted the initiation and faster propagation of stress cracks. Thermal results shows that the thermal conductivity of the hardened mixture is almost linearly proportional to the density of the specimen. The porosity brought by FAC made the thermal conductivity of the concrete decrease. The study found the thermal conductivity of lightweight concrete with coarse light weight aggregates and 50% sand replaced by FAC is around 0.71-0.85 W/m K.

Sarpathy et. al [13] reckon that further research on developing a lightweight concrete using both fly ash cenosphere and fly ash is needed. In their study, fly ash cenoshpere and sintered fly ash replaced natural fine aggregate and coarse aggregate respectively. The study discussed on workability, fresh density, dry density, compressive strength, split tensile strength, flexural strength, water absorption and volume of permeable pore space with different amount of FAC and SFA replacing NFA and NCA. Results shows that all fifteen concrete mixes with different combination of FAC and SFA satisfy requirement of structural lightweight concrete based on ACI 213R-03. As the amount of FAC and SFA increases, the general strength of the lightweight concrete decreases. The compressive, split tensile, flexural and bond strength are found to be within the range of 19.35–32.04 MPa, 1.83– 3.48 MPa, 1.81–4.27 MPa and 6.95–8.33 MPa, respectively. From compressive, tensile and flexural strength tests, the study concluded that the optimum amount combination of FAC and SFA is 50% of NFA replaced by FAC and 75% of NCA replaced by SFA. This combination constantly yields relatively the

highest strength in most of the tests. The water absorption rate of the mixture increases as the dry density of the concrete decreases. Researchers suggests that the high amounts of lightweight aggregate create more hollow space to absorb water. They also point out that both FAC and SFA have relative high water absorption rate and they need add extra water during mixing.

Patel et al. [14] investigate the development of lightweight concrete by replacing the natural fine aggregate (NFA) with an industrial waste called fly ash cenoshperes (FAC). In their study, Patel et al. prepared one control mix and another ten mixes by replacing 20%, 40%, 60%, 80% and 100% of NFA with FAC. The workability and fresh state density of the lightweight concrete with varying amount of FAC replacement were investigated. Oven density of the developing lightweight concrete is also studied. The mechanical testing includes compressive strength tests, split tensile strength tests and flexural strength tests. Finally, water absorption and volume of permeable voids of the lightweight concrete are investigated. Results indicate that slumps of the fresh concrete mixes decrease as FAC replacement increases. The fresh and oven dried density of the lightweight concrete present a similar trend. For compressive strength, increase of FAC replacements dramatically reduce the strength. Tensile and flexural strength of lightweight concrete also reduce as the replacement of FAC increases, but not as greatly as compressive strength. On the contrary, both water absorption and volume of permeable voids of the lightweight concrete increase along the increase of FAC replacement.

Hanif et al. [15] studied the effect of nano silica (NS) on the properties of cement pastes incorporating fly ash cenospheres (FACs). FAC was used to replace 10%, 20% and 30% of cement in the mix. Nano silica is utilized to enhanced the mechanical properties of FAC incorporating lightweight concrete. This study investigated the effect of FAC and NS on the mechanical properties of lightweight concrete by conducting compressive strength tests and

microstructure analysis of the specimens. Porosity of the lightweight concrete is also studied. Results indicate that FAC replacement reduce the compressive strength of the lightweight concrete almost linearly. With the addition of NS, compressive strength reduction from FAC replacement can be deducted. The enhancement on compressive strength with NS addition is more distinctive when the specimens reached 7-days and 28-days age. However, the enhancement effect is less obvious with specimens reach ages of 56-days and 90-days. Porosity increases with the replacement of FAC. NS addition reduced the porosity in the pastes. However, with longer age, the effect of NS addition was minimal.

Rheinheimer et al. [16] conducted an integrated multi-scale study of high-strength low-thermal conductivity cement composites containing cenoshperes. Their study investigated thermal conductivity and mechanical properties of cenoshperes containing composites. In addition, microscopic investigation and numerical simulations also are conducted. Results shows cenoshperes inclusion in the cement composites reduces about 50% of the thermal conductivity of cement composites. Addition of cenoshperes did not affect the compressive strength. The numerical simulations on thermal conductivity also agree with the experimental results.

2.2 3D printable lightweight cement composites

3D concrete printing is a promising technology in construction industry. However, there certain requirements for concrete materials to be printable. 3D printing concrete materials should have good flowability to ensure a continuous concrete filament during printing while also having capacity to resist loads caused by subsequent printing layers without large deformation. Therefore, there have been a large number of studies on studying fresh and rheological properties of printable concretes. A few of these studies have focused on the development of lightweight printable concrete materials.

Zhang et al. [17] conducted a study on rheological and harden properties of the high-thixotropy 3D printing concrete. High-thixotropy 3D printing concrete based on five different level of sand to cement ratio (S/C) at 0.6, 0.8, 1.0, 1.2 and 1.5 was developed. The thixotropic compositions used in this study were nano clay (NC) and silica fume (SF). The water to cement ratio (W/C) is 0.35. A water reducer, thicker agent and fine aggregate (river sand) also were utilized. The workability of the mixtures was assessed via the drop table test. Rheological properties were systematically evaluated using a concrete rheometer. Two optimal mixes were selected to further study the hardened properties of the 3D printed concrete. Concrete blocks were printed then cut into required size for compression tests, flexure tests and drying shrinkage tests. Specimens were placed into a constant temperature and humidity condition for curing. Mechanical properties of the specimens were studied after 28 days of curing. Rheological test results show the sand to cement ratio is almost linearly correlated to both viscosity and yield stress, i.e., viscosity and yield stress increase as the S/C ratio increases. Thixotropy has an inverse correlation with S/C ratio, i.e., thixotropy decrease along the increase of S/C ratio. The relationship between open time and rheological properties was investigated with S/C ratio from 0.6 to 1.2. The fresh mixture with S/C ratio of 1.5 could not be sheared due to its high stiffness. Results show that increase in open time cannot influence viscosity and yield stress significantly. Mixture with S/C ratio at 1.0 and 1.2 was identified at the optimum for pumpability, extrudability and buildability. Mechanical tests show that S/C ratio has a little effect on compressive and flexural strength of the mixture. The dry shrinkage rate of printed concrete with S/C ratio at 1.0 and 1.2 agrees with previous studies after 70 days. The capacity to resist drying shrinkage of 3D printing concrete developed for this study was noticeably stronger than that of sprayed concrete.

Weng et al. [18] investigated utilizing Fuller Thompson theory and Marson-Percy model to design 3D printing cementitious materials. 3D printable cementitious materials have special requirements for rheological properties. Fuller Thompson theory and Marson-Percy model are tool to optimizing sand gradation and packing fraction. Weng et al. states that a continuous grading system with less voids will increase the contact points between particles which leads to better flowability of the cementitious materials. Several different sand gradation systems were utilized. Rheological results shows that mixture with continuous gradation based on Fuller Thompson theory and Marson-Percy model produced the best result for 3D printing. The actual printing tests also confirmed the rheological results. Mixture with continuous gradation was able to be printed for most amounts of layers before collapse.

Falliano et al. [19] studied fresh state stability and mechanical strength of 3D-printed lightweight foamed concrete. Lightweight foamed concrete consisted of cement paste and appropriate preformed foam. In this study, the difference between 3D-printed foamed concrete and classical foamed concrete was studied. An extrusion test was used instead of a cone test to determine the stability difference between 3D-printed foamed concrete and classical foamed concrete. Result indicates that 3D-printed foamed concrete hardly deformed at its fresh state compared to classical foamed concrete. The study stated that viscosity enhancing agent is acting like bridges or connections between the cement particles and increasing the yield stress of the material. For mechanical properties, this study evaluated the effect of targeted dry density, cement type, water/cement ratio, curing conditions and mixing intensities on the compression and flexural strength. Result clearly showed that dry density and mechanical strength has an almost linear relationship. In particular, compressive strength increases with an increase in dry density. A low water/cement ratio yielded a higher compressive strength. A better curing

condition generated a more consistent results and higher compressive strengths. The study also found that 3D-printed lightweight foamed concrete has higher compressive strength than that of classical lightweight foamed concrete. They concluded that the smaller and more evenly disturbed air bubble increased the compressive strength of 3D-printed lightweight foamed concrete compared to its classical counterpart. Surprisingly, mixing intensities showed the most dramatic difference in results among all the variables. The study stated that the more intensive mixing yielded smaller air bubbles, resulting a higher compressive strength.

Ting et al. [20] investigated the use of recycled glass as the fine aggregates for 3D concrete printing applications. Incorporating crushed recycled glass into construction materials can reduced the effort of recycling glass. In their study, recycled glass was used to replace fine aggregate. The rheological and mechanical properties of the concrete incorporating recycled glass are examined. Results indicate that, comparing to printable concrete with sand aggregate, static yield stress of the printable concrete with recycled glass reduced greatly which can lead to potential poor buildability for 3D printing. The dynamic yield stress and plastic viscosity of the concrete utilizing recycled glass also reduce comparing to printable concrete utilizing sand aggregates which shows that concrete with recycled glass has better flowing properties. Compressive strength, flexural strength and splitting tensile strength of the concrete composite all reduce with the fine sand aggregate replaced by recycled glass.

Cuvas et al. [21] further investigated the rheological properties of 3D printable lightweight cementitious composites with incorporated waste glass aggregate and expanded thermoplastic microshperes (ETM). Mixes with 0 vol.%, 50 vol.% and 100 vol.% of sand replaced by waste glass were prepared. More mixes incorporating ETM were prepared as well with same volume replacement of waste glass above. Besides rheological tests, a set of

specimens is printed to evaluate the shape retention abilities of the composites. Results shows that both waste glass replacement and ETM have effect on the rheological properties of the mixtures. However, different tests deliver different trends. Cuvas et al. state that possible cause is due to the spherical shape of the ETM particle which facilitate the transition of the cement paste when subjected to shear. Shape retention test results shows that the addition of ETM can positively affect the printing parameters and improve buildability of the printed concrete composites.

2.3 Rheology measurement method

Rheological properties are measured with a rotational viscometer. Rotational viscometer measures the torque that arises from the flow resistance of the sample. Then, shear force can be calculated from the torque measurement. The two-plates model is used to define rheological parameters as shown in Figure 3 [22]. Shear is applied to a sample

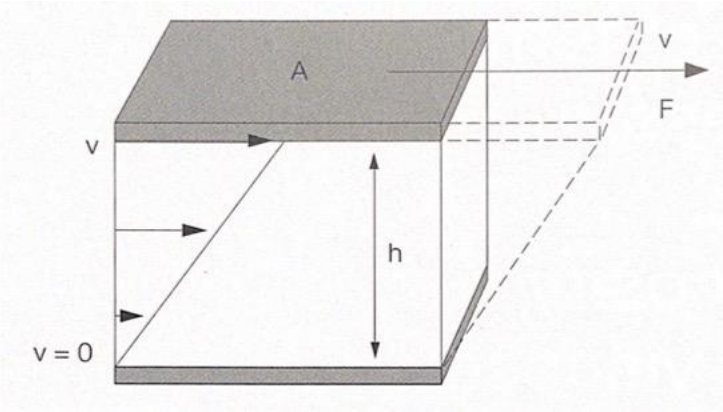

Figure 3. Two-plates model for shear test with shear area *A*, gap width *h*, shear force *F* and velocity *v* [22]

sandwiched between two plates. The lower stationary plate is mounted on a rigid support and the upper plate can be moved parallel to the lower plate. The rheometer measure shear force via torque at each measuring point, then calculate shear stress, shear rate and viscosity of the sample.

Shear stress τ can be calculated using equation as follow, where *F* is the shear force and *A* is the shear area:

$$\tau = \frac{F}{A}$$

Shear rate γ can be calculated using equation as follow, where *v* is the flow velocity of the sample and *h* is the shear gap between two plates:

$$\gamma = \frac{v}{h}$$

Viscosity η is defined as shear stress τ divided by shear rate γ. Viscosity can be calculated with equation:

$$\eta = \frac{\tau}{\gamma}$$

2.4 Thermal conductivity measurement method

There are various methods to measure thermal properties of composite materials. In this study, a testing method for measuring steady-state thermal transmission properties with heat flow meter apparatus was employed. Heat flow meter (HFM) apparatus is relatively simple and applicable to a wide range of test specimens. With proper calibration, the precision of the heat flow meter is excellent [23]. Specimen is placed in between a hot plate and a cold plate with two heat flux transducers in the center of the two plates. Heat flow vertically through the specimen [24]. Figure 2 demonstrate the working principle of a heat flow meter.

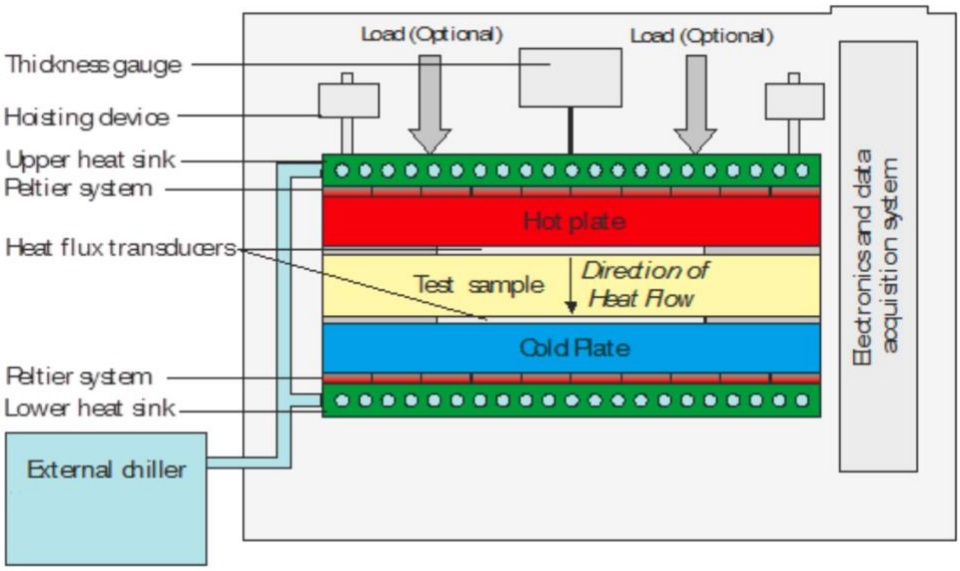

Figure 4. Measuring principle for the heat flow meter [24]

Heat flux q (W/m^2) is defined as the rate of heat flow Q (W) through a specific area A (m^2) of the sample. Heat flux transducers, shown in Figure 4, produce a voltage V that is proportional to the heat flux. The heat flux is calculated using the Fourier heat flow equation:

$$q = \frac{Q}{A} = \lambda \frac{\Delta T}{\Delta x}$$

Where λ is the thermal conductivity of the sample, ΔT is the temperature difference across the sample, Δx is the thickness of the sample, A is the area through which the heat flows. The HFT voltage output V is proportional to the heat flux q in the heat flow transducers metering area. A constant of proportionality N can be used to convert the voltage signal to heat flux with the equation following:

$$q = N \cdot V$$

The calibration factor N is determined by separate calibration runs using a reference standard specimen with known thermal conductivity values. Combining equation (1) and (2) and solving for thermal conductivity produces equations following:

$$\lambda = k = NV\frac{\Delta x}{\Delta T}$$

3. EXPERIMENTAL METHODS

3.1 Materials

In this study, ordinary Portland cement type I/II and high early strength cement (cement type III) were used with the conformation to ASTM standard C150 [25]. In addition to the Portland cement, binder also contains silica fume (SF). Due to its fine nature, silica fume was used to effectively fill the empty pores to produce a stronger and more compact material. The water to binder ratio was 0.32. Sand with a particle size ranging from 0.15mm to 0.6mm was used as natural fine aggregates. In order to reduce the drying shrinkage, expansive agent was utilized in the mixes. A water reducer (WR) was utilized to improve the workability of the mixtures. Besides sand, all materials described above were kept constant in all mixes.

One of the main variables in test matrix for this study is the content of fly ash cenoshperes (FACs). FACs were used to replace sand to at a select amount in all mixes. FACs are hollow ceramic sphere particles with true density less than 0.85 g/cm^3. The particle size of the FACs used in this study ranges from 10 to 106 microns. Particle distribution of FACs is shown as Table 1 which is provided by the manufacturer (Cenostar Corporation).

TABLE 1. Particle size distribution of FACs

Size (microns)	Percentage
<106	97% (<3% over)
75 - 105	35% - 47%
45 -74	20% - 39%
<44	5% - 11%

Figure 5 shows a Scanning Electron Microscopy (SEM) image of FACs. It can be seen that the FACs particles are spherical and hollow with diameter ranges from 10 to 50 microns.

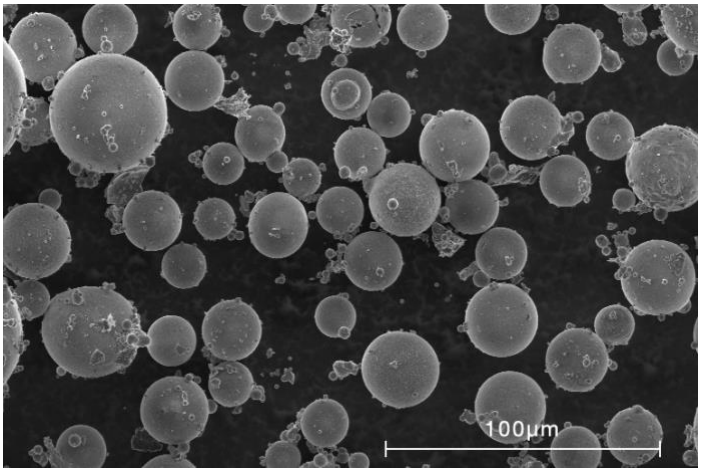

Figure 5. SEM image of FACs particles

The other variable in the test matrix is the ratio of viscosity modifying agent (VMA). VMA is a water-soluble polymer which can fix some of water molecules to the periphery of chain and thereby increase the viscosity of solution [26]. VMA was used to increase the viscosity and improve the printability of the mixture.

3.2 Mixture preparation

A total of 16 mixtures were prepared for rheological, thermal and compressive testing. Three samples were prepared for each test. About 500 ml of material was prepared for the rheological measurement, which were conducted right after mixing. Time gap between the end of mixing and start of rheological measurement was 1 min for each sample to ensure consistency. For thermal conductivity measurements, three specimens with a size of 203 x 203 x 51 mm were prepared for each mix. Cubic specimens with a side length of 50 mm were prepared for compression tests.

Table 2 shows that material proportions for sixteen mixtures. In this study, FACs was used to replace 0, 20, 40 and 60 volume percentage (vol. %) of sand. The variation of VMA was

also set at four level at 0%, 0.1%, 0.2% and 0.3% of the weight of the binder. Table 3 shows the variation of two factors and their corresponding levels.

TABLE 2 Full mix design (kg/m^3 of mortar)

Mix ID	Materials at constant amount						Materials at varying amount		
	Binder								
	Cement	C III	SF	EA	Water	WR	Sand	FACs	VMA
Mix 1	798	90	100	30	316	15	1000	0.0	0.0
Mix 2	798	90	100	30	316	15	1000	0.0	1.0
Mix 3	798	90	100	30	316	15	1000	0.0	2.0
Mix 4	798	90	100	30	316	15	1000	0.0	3.0
Mix 5	798	90	100	30	316	15	800	64.5	0.0
Mix 6	798	90	100	30	316	15	800	64.5	1.0
Mix 7	798	90	100	30	316	15	800	64.5	2.0
Mix 8	798	90	100	30	316	15	800	64.5	3.0
Mix 9	798	90	100	30	316	15	600	129.0	0.0
Mix 10	798	90	100	30	316	15	600	129.0	1.0
Mix 11	798	90	100	30	316	15	600	129.0	2.0
Mix 12	798	90	100	30	316	15	600	129.0	3.0
Mix 13	798	90	100	30	316	15	400	193.5	0.0
Mix 14	798	90	100	30	316	15	400	193.5	1.0
Mix 15	798	90	100	30	316	15	400	193.5	2.0
Mix 16	798	90	100	30	316	15	400	193.5	3.0

TABLE 3 Experiment factors (variables) in four levels

Levels	FACs%	VMA/b
Level 1	0.0%	0.0%
Level 2	20.0%	0.1%
Level 3	40.0%	0.2%
Level 4	60.0%	0.3%

To prepare the specimens, the binder (cement type I/II, cement type III and silica fume) was first dry mixed using a 20-quart capacity Hobart HL 200-10STD planetary floor mixer for 30s at 107 rpm speed. Then, sand, expansive agent and FACs were added into the mix and mixed

for another 30 seconds. The required amount of WR and VMA were mixed with water into a water solution. Then, the solution was added into the mixer. Mixing procedure was paused for 30 seconds to allow dry mixture to absorb water. After pausing, mixing resumed at low speed for 30 seconds. After 30 seconds, mixing was paused again. During this time, mix was scraped down manually in order to allow any paste that may sticked on the side or at the bottom of the mixing bowl to be mixed properly. Finally, mixing resumed for 60 seconds or longer at medium speed (198 rpm) to achieve a homogenous mixture.

2^k full factorial design of experiments (DoE) was carried out, where 2 represents the number of factors and *k* represents the number levels, to analyze the effects of these factors in the results. Four level factorial design ($k = 4$) was selected to analyze the main effects and the interaction effects of the variables on the response variables. Table 4 shows the full factorial design with two variables and four levels for each variable. Analysis of Variance (ANOVA) was carried out in order to measure the effects of main factors (FACs replacement ratio and VMA/b ratio) and their interaction.

TABLE 4. Full factorial design

Mixes	1	2	3	4	5	6	7	8	9	10	11	12	13	14	15	16
FACs%	1	1	1	1	2	2	2	2	3	3	3	3	4	4	4	4
VMA/b	1	2	3	4	1	2	3	4	1	2	3	4	1	2	3	4

3.3 Rheology Testing Method

For the rheological measurements, Anton Paar MCR 301 rheometer was used which is capable of measuring the torque values ranging from 1 nNm to 200 mNm. Since the rheometer is considerably sensitive at even very low shear rates, motor adjustments were made before starting the tests to minimize the residual forces. Shear rate controlled rotational measurement was

applied for all tests where a fixed displacement was applied to the sample at a constant velocity and the torque required to achieve that displacement was measured. The measurements were performed with a specially designed building cell (BMC 90) container together with a stirrer vane. The building cell has a cylindrical geometry with dimensions of 70 mm in diameter and 90 mm in height and requires approximately 400 ml of mortar for each run. The building cell includes an inner cage to prevent slippage of samples. The stirrer vane is connected to the coupling of the rheometer and applies counter clockwise rotations to the mortar sample for the measurements. The gap between the stirrer and the inner cage of the building cell is 6 mm and this is the place where shearing is established. Figure 6a shows the rheological test setup with loaded sample and Figure 6b shows the schematic representation of the building cell with stirrer vane.

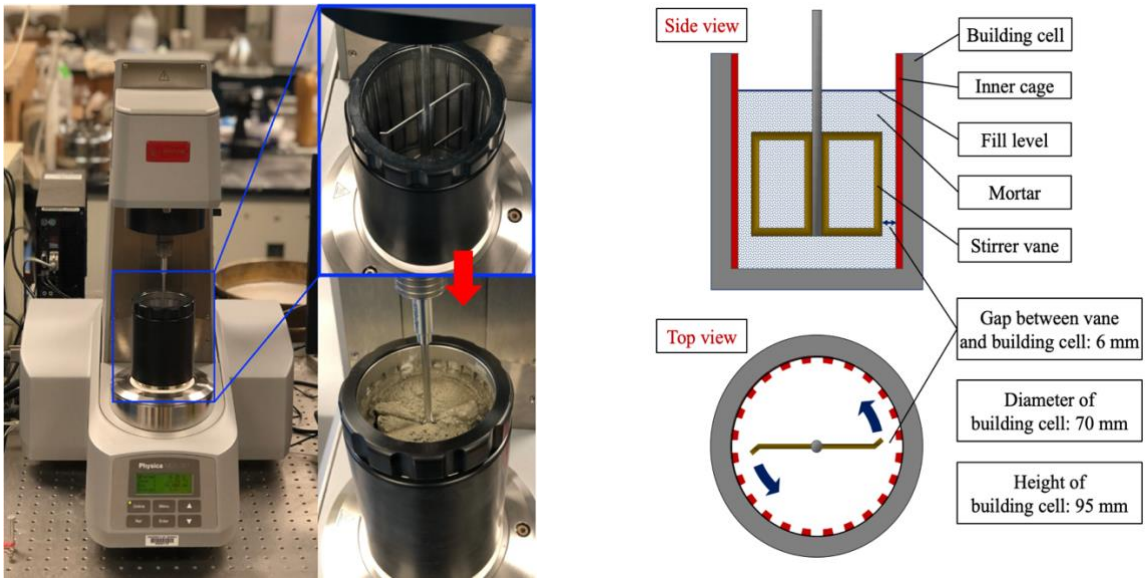

(a) (b)

Figure 6. (a) Rheometer, empty building cell with stirrer vane and freshly poured mortar in the building cell, and (b) schematic representation of side and top views of the building cell.

Stress growth tests were conducted to determine the yield stress and the apparent viscosity. In particular, a shear rate-controlled test protocol was performed for all mixes where a constant shear rate of 0.1 s^{-1} was applied for 60 s (Figure. 7(a)). With this applied shear rate, the corresponding shear stress values were recorded by the rheometer. For each test, the stress values have a period of rapid increase, followed by a period where the growth significantly slows down but continues to increase slightly. A linear regression model was fitted on the increasing stage of each test as shown in Figure 4b for mix 1. The range of this linear stage is defined as Δt which is calculated by $(t_f - t_s)$, where t_f refers to the finishing time of the test (60 s for each test) and t_s refers to the starting time of the linear range and located where more than 3% difference was observed between linear fit and actual test results from 60 s to 0 s. The average of measured shear stresses in this time interval Δt is calculated as the yield stress of the material. The apparent viscosity was also obtained from the rheometer measurements as the ratio of the shear stress to the shear rate.

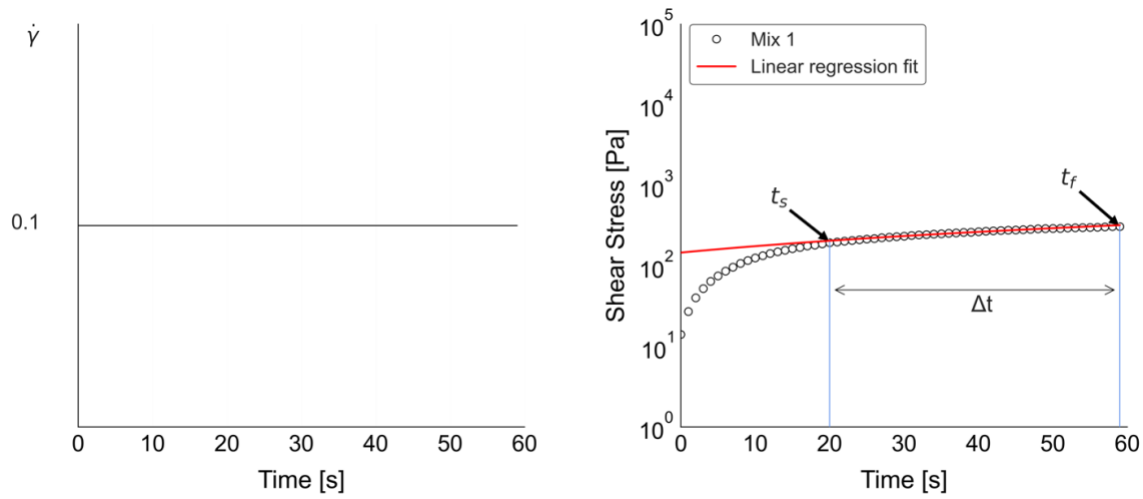

(a) (b)

Figure 7. (a) Test protocol for rheological measurements, and (b) shear stress test result for Mix 1 with yield stress calculation method

3.4 Compressive strength testing method

Compression strength tests followed ASTM C109 [27] standard testing method. For compression tests, 50 mm cubic specimens were casted and water cured for 28 days in room temperature. After 28 days of water curing, specimens were tested at a loading rate of 689.5kPa/s. A scanning electron microscopy (SEM) analysis was also conducted on a selected of mixtures. SEM samples were acquired from the failed compression specimens.

3.5 Thermal conductivity testing method

Thermal conductivity of developed FAC-based cementitious composites were measured using a heat flow meter (NETZSCH HFM446). This equipment follows the guidelines provided in ASTM C518 [22]: Standard Test Method for Steady-State Thermal Transmission Properties for thermal conductivity measurement. Specimens with a size of 203 mm × 203 mm × 51 mm (Figure 8(a)) were casted and water cured for 28 days in room temperature. After 28 days of

water curing, specimens were air dried for 7 days, then oven dried until they reached a constant weight. For this study, when the percent difference in weight between two last measurements was less than 1%, the specimen was considered reaching at a constant weight. During thermal conductivity tests, the upper plate of the heat flow meter was set at 30 degrees Celsius and the lower plate was set at 10 degrees Celsius. This setting created a 20 degrees Celsius difference and a median temperature of 20 degree Celsius which simulate normal room temperature. Since cementitious composites are considered to have a relatively high thermal conductivity and also the specimens might have rough surface, two rubber interface sheets and two thermal couples were used during the testing to ensure the accuracy of the results as shown in Figure 8(b). In addition, a 2 kPa pressure was applied to the specimens to ensure the specimens' surfaces were fully contacted with the heat flux sensor.

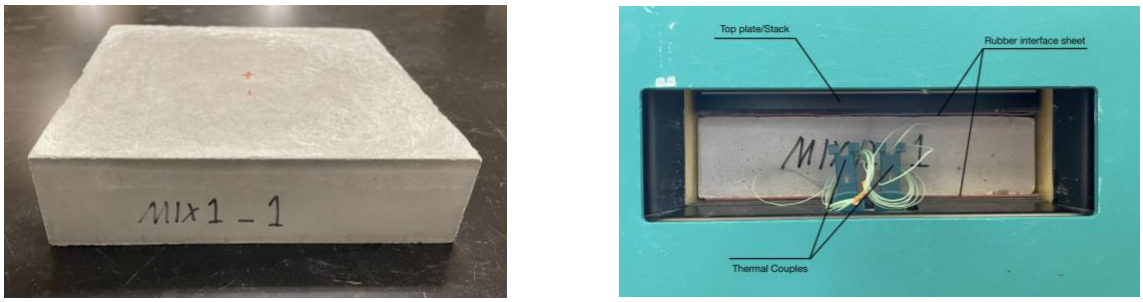

(a) (b)

Figure 8. (a) Thermal specimen and (b) test set-up

3.6 Buildability Testing Method

A 3D printer with screw-based extrusion behavior (Figure. 9) was used for the printability and buildability of the most promising mixture proportion. Two different types of nozzles were used; one L-shape rectangular cross-section (30 mm×15 mm), where a horizontal extrusion was performed, and one circular cross-section (16 mm in diameter), where a vertical

extrusion was performed (Figure. 9). Shape stability of the selected mix was analyzed by printing a lab-scaled version of a target structure with rectangular nozzle, whereas, buildability was measured as the maximum printable layers with the circular nozzle.

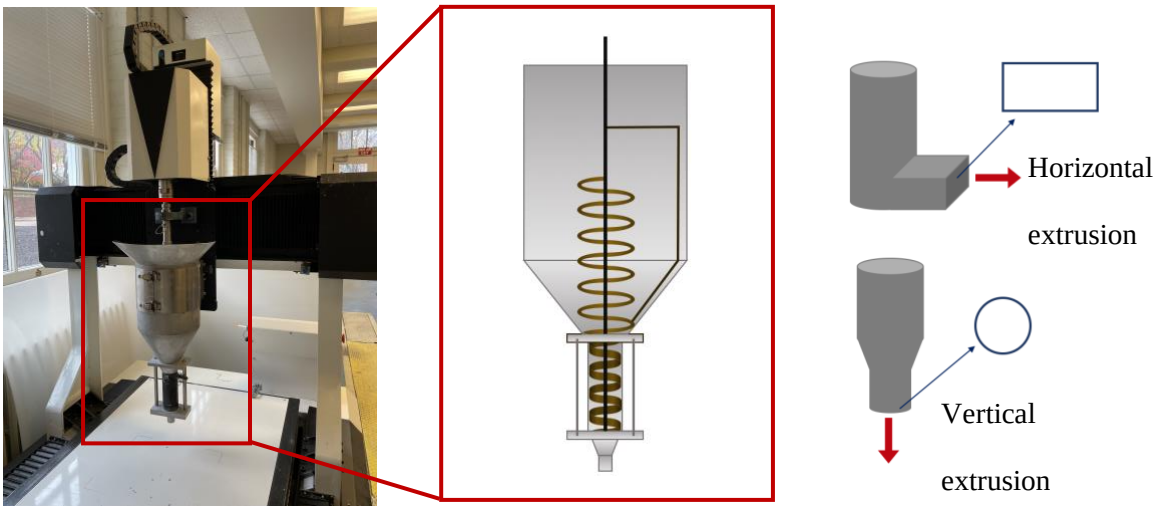

Figure 9. 3D printer with screw-based extrusion and nozzle types

A direct printing testing method proposed by Nerella [28] was used to assess buildability of the mixtures considering a target application. In this method, since the verification of the successful buildability of the full-scale structure is practically and economically unfeasible, a lab-scaled version of the target application is printed in laboratory. The target application for this study was selected to be a 3D printed one story residential building fabricated with lightweight cementitious concrete. If the total height and the breadth (thickness) of a representative wall in the target structure are H_{target} and B_{target}, respectively, then the aspect ratio of the representative wall is defined as:

$$A_t = \frac{H_{target}}{B_{target}} \quad (1)$$

Then, the total height of the lab-scaled structure (H_{theo}) can be calculated using the breadth of the wall (B_{theo}) as:

$$H_{theo} = A_t \times B_{theo} \quad (2)$$

If the height of a single layer is h_{theo}, then the number of layers aimed to print the lab-scaled version of the target structure is;

$$n_{layers} = \frac{H_{theo}}{h_{theo}} \quad (3)$$

Combining equations (2) and (3) gives;

$$n_{layers} = \frac{A_t \times B_{theo}}{h_{theo}} \quad (4)$$

Note that the equations above give the dimension calculations of the structure before printing, hence theoretical variables, and the dimensions after printing are regarded as experimental measures. The total height of the experimentally printed structure (H_{exp}), the breadth of each layer $B_{exp,i}$ as well as the height of each layer ($h_{exp,i}$) are measured and discussed in the results section.

A common residential building with a wall height of 2.5 m and wall thickness of 0.25 m as described in the "Guide to Residential Concrete Construction" (ACI 332.1R-06 [29]) was selected as target application. Given this information, the dimensions of the walls to be printed in the laboratory are calculated using the equations (1)-(4), and summarized in table 5.

TABLE 5 Dimensions of target and lab-scaled structure and parameters for buildability test

	Parameters	Values
Target Wall	Height, H_{target}	2.5 m
	Width, B_{target}	0.25 m
	Aspect ratio, A_t	10
Experimental Wall	Height, H_{theo}	300 mm

Rectangular Nozzle	Layer Width, B_{rect}	30 mm
	Layer Width, H_{rect}	15 mm
	No of layers, n_{layers}	20
Circular Nozzle	Layer Width, B_{rect}	16 mm
	Layer Width, H_{rect}	13 mm
	No of layers, n_{layers}	23

Time gap between the printed layers effects the bond strength between the layers as studied by researchers. Tay et al. [30] studied the time gap effect on the bond strength of the 3D-printed concrete and observed that the increase in time gap between the layers resulted in decrease in direct tensile strength between the layers. In another study, Panda et al. [31] showed that the yield stress and viscosity increase with increased time gap between the layer, which is favorable for shape stability, however, they also showed that the bond strength between the layers decreases with increased time gap. Since the scope of this study is not an in-depth analysis of time gap, a time gap of 60 s between the layers was used during direct printing tests.

4. EXPERIMENTAL RESULTS

4.1 Rheology Results

Figure 10 shows the results obtained from stress-growth tests. For each of 16 mixtures, the variation of shear stress with time are plotted as the mean results of three tested specimen while the standard deviations at each measurement time are given on the curves. It can be seen that shear stress increases rapidly during each test and then tends to remain constant. Using the mean shear stress – time curve, the static yield stress for each mixture is computed as described in the earlier section.

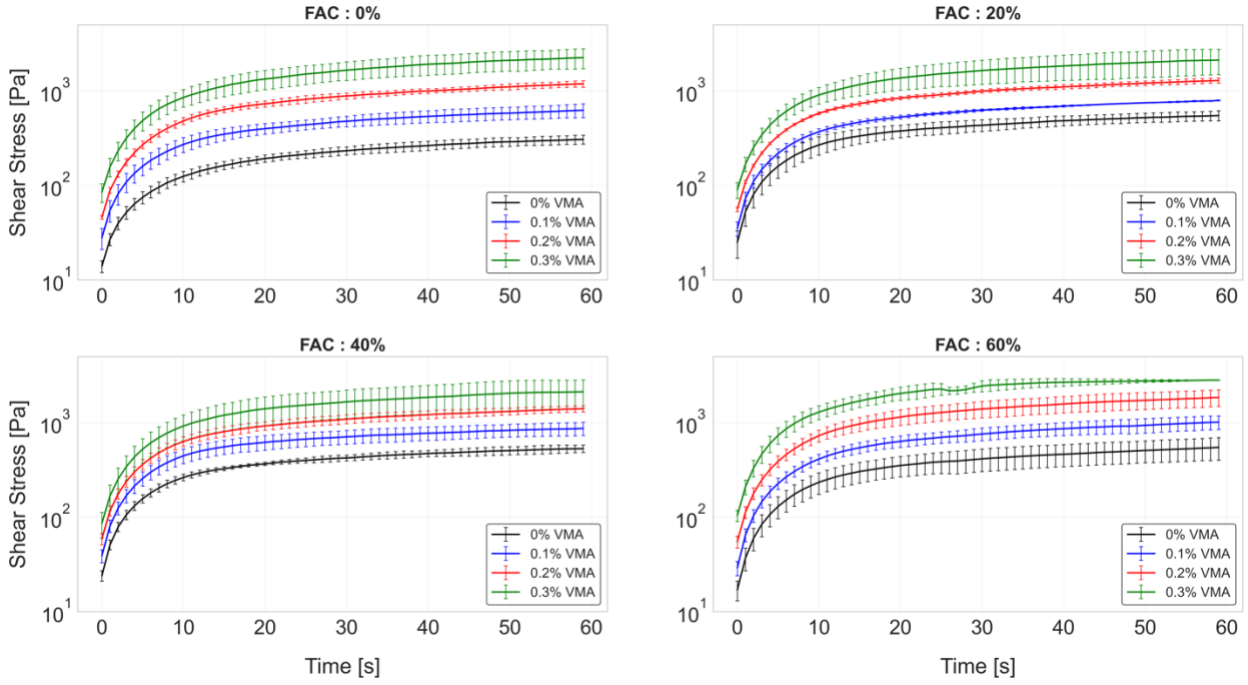

Figure 10. Shear stress – time curves for all mixtures

Figure 11(a) shows the static yield stress values of all sixteen mixtures. The results are represented in a heat map where the values are depicted by color distribution, hence, makes it easy to visualize the factorial design experiments. It can be seen from figure 11a that the increase in the yield stress with an increase in FACs content, for a constant VMA/b ratio (i.e., vertical

color change), is not significant. On the other hand, significant increases in the yield stresses were observed for an increase in VMA content at any level of FACs content (i.e., horizontal color change). In particular, the yield stress for the control mix (level 1 for both FACs and VMA/b) was measured as 259 Pa. Keeping VMA/b at 0% and increasing the FACs content from 0% to 20% increased the yield stress from 259 Pa top 468 Pa, which is 81% improvement. However, further increase in FACs content at 0% VMA/b did not help increase the yield stress, but slightly decreased it to 459 Pa and 452 Pa for 40% and 60% FACs replacement ratios, respectively. On the other hand, the effect of VMA on the yield stress was considerably high at all levels of FACs contents. At level 1 of FACs replacement %, for instance, the yield stresses were measured as 523 Pa, 973 Pa and 1870 Pa for the VMA/b levels of 2, 3 and 4, respectively, indicating 102%, 276% and 622% increases compared to the mixture without any VMA, respectively. Also, note that since the shear rate was constant during the rheology tests, the same effects for the two test factors (FACs replacement % and VMA/b %) was observed on apparent viscosity and yield stress.

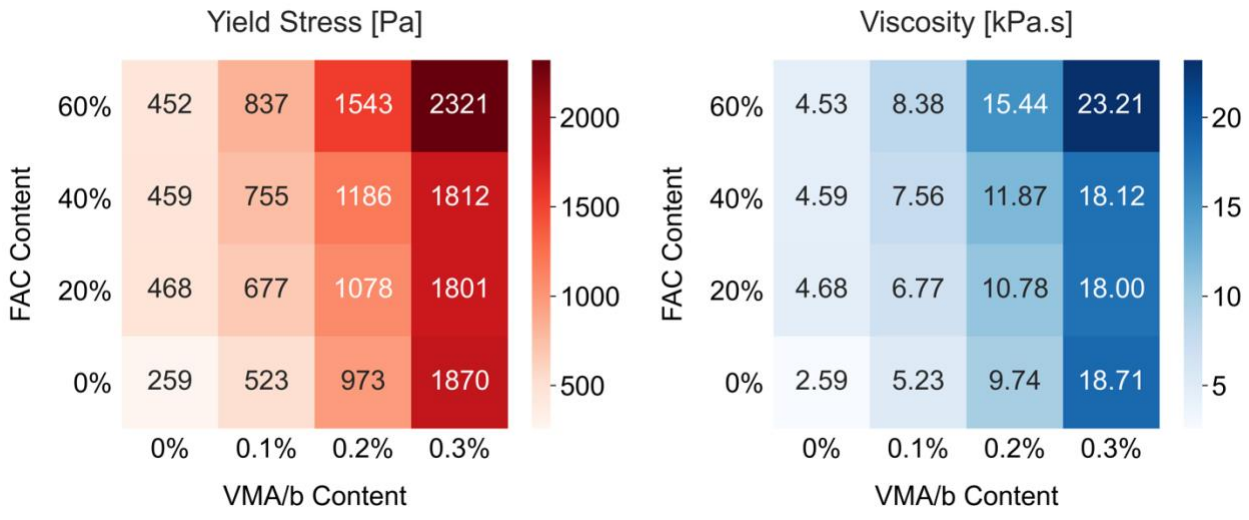

(a) (b)

Figure 11. (a) Yield stress and (b) Viscosity for all mixtures

In order to further assess the effects of the factors on the yield stress, a linear regression model was fit on the data and the results are represented in Figure 12. Figure 12(a) shows the variation of yield stress with respect to FACs content and the corresponding regression line is represented in red dashed line. Data points are observed to be apart from the regression line for each level of FACs content, which resulted in only 0.05 of R^2 (coefficient of determination). This result shows that the response variable, i.e., yield stress, does not have a correlation with the FACs content. On the other hand, the data points are considerably close to the regression line at Figure 12(b) where the variation of the yield stress with the VMA/b ratio is plotted. The R^2 of the result of the regression model was 0.89. Thus, yield stress and viscosity of the mixture have positively correlation with the VMA/b ratio, i.e., yield stress and viscosity of the mixture increase as the increase of VMA/b ratio. The long-chain molecules of VMA absorb and fix part of the mix water [26]. Molecules in adjacent polymer chains develop attractive forces which block further water migration, resulting the increase of viscosity in the mixture.

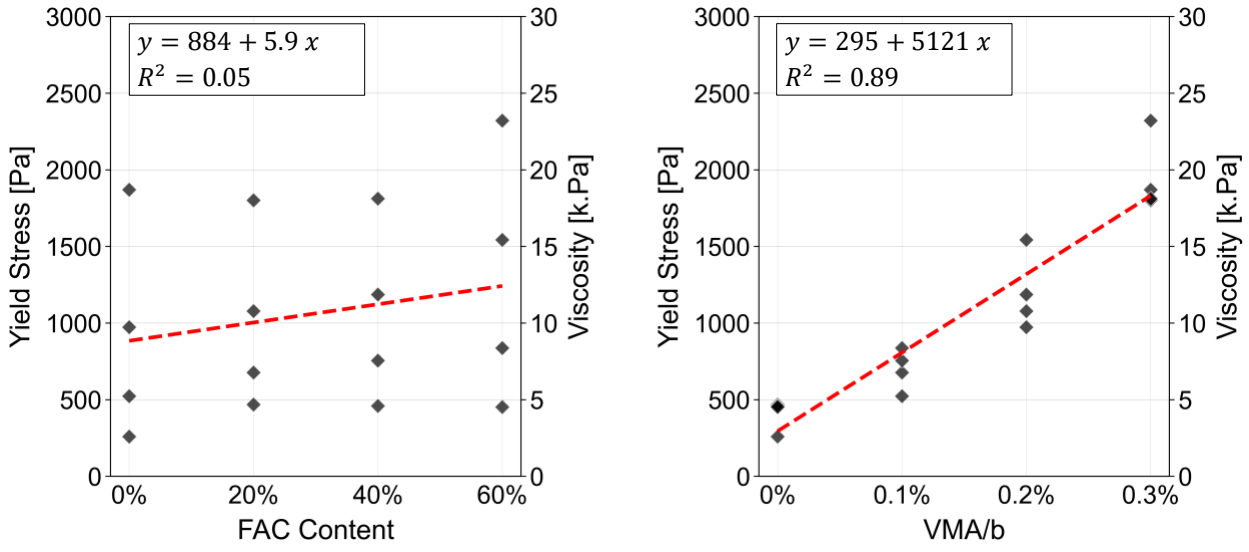

(a) (b)

Figure 12. The variation of yield stress with; (a) FACs content and (b) VMA/b ratio.

The effects of selected factors on yield stress were also analyzed with ANOVA as shown in table 6. For a factor to be significant on the response variable, the *p-value* of the corresponding factor should be smaller than 0.05 (critical value) which corresponds to 95% of confidence level. Besides the main affects (FACs replacement % and VMA/b %), interaction effect of these factors is also included in the analysis. Since the *p-values* for the FACs only and its interaction with VMA/b factor are considerably higher than the critical value, it can be concluded that the FACs content is not significant on yield stress. The only significant term in the ANOVA table was recorded as VMA/b content which has the *p-value* of 0.016. This indicates the VMA/b ratio is the only factor that is significant in the yield stress variation.

TABLE 6. ANOVA analysis results

Variables	Sum of Squares	Degrees of Freedom	F-Value	p-value	Significance
FACs	65694	3	0.730	0.598	Not Significant
VMA/b	1636196	3	18.197	0.019	Significant
FACs * VMA/b	48865	6	0.272	0.918	Not Significant
Residual	89913	3			

4.2 Compressive Strength Results

The compressive strength test results for each specimen are shown in Table 7.

TABLE 7. Compressive Strength of cubic specimens with varying FACs Content and VMA Ratio

Batch	Specimens	FACs Content	VMA Ratio	Compressive Strength (Mpa)	Average
Mix1	1	0%	0.0%	59.77	62.05
	2	0%	0.0%	59.29	
	3	0%	0.0%	67.09	
Mix2	1	0%	0.1%	65.54	70.68
	2	0%	0.1%	70.37	
	3	0%	0.1%	76.12	
Mix3	1	0%	0.2%	70.71	67.78
	2	0%	0.2%	66.11	
	3	0%	0.2%	66.51	

Mix4	1	0%	0.3%	61.39	53.97
	2	0%	0.3%	57.78	
	3	0%	0.3%	42.73	
Mix5	1	20%	0.0%	51.15	49.59
	2	20%	0.0%	52.91	
	3	20%	0.0%	44.71	
Mix6	1	20%	0.1%	59.55	59.87
	2	20%	0.1%	52.17	
	3	20%	0.1%	67.91	
Mix7	1	20%	0.2%	53.99	48.46
	2	20%	0.2%	48.34	
	3	20%	0.2%	43.05	
Mix8	1	20%	0.3%	45.65	45.06
	2	20%	0.3%	47.66	
	3	20%	0.3%	41.88	
Mix9	1	40%	0.0%	59.04	56.75
	2	40%	0.0%	52.63	
	3	40%	0.0%	58.58	
Mix10	1	40%	0.1%	51.39	50.35
	2	40%	0.1%	39.74	
	3	40%	0.1%	59.91	
Mix11	1	40%	0.2%	39.83	47.50
	2	40%	0.2%	47.90	
	3	40%	0.2%	54.76	
Mix12	1	40%	0.3%	43.36	49.76
	2	40%	0.3%	51.94	
	3	40%	0.3%	53.98	
Mix13	1	60%	0.0%	49.95	47.05
	2	60%	0.0%	43.30	
	3	60%	0.0%	47.90	
Mix14	1	60%	0.1%	45.22	40.56
	2	60%	0.1%	40.16	
	3	60%	0.1%	36.31	
Mix15	1	60%	0.2%	41.15	43.50
	2	60%	0.2%	46.15	
	3	60%	0.2%	43.20	
Mix16	1	60%	0.3%	36.51	43.52
	2	60%	0.3%	49.48	
	3	60%	0.3%	44.55	

Figure 13 shows the average compressive strength of all the developed mixtures. The results are grouped based on the VMA/b ratios and plotted for varying content of FACs. In addition, Figure 14 shows the variation of compressive strength individually with FACs contents and VMA/b ratio. It can be seen the mixtures without any FACs always have higher compressive strength than the mixtures with FACs. For a select VMA/b ratio, increasing the FACs ratio usually decreases the compressive strength. This correlation and the rate in decrease is strongest for the specimens with 0.1% VMA/b ratio. For both 0% and 0.3% VMA/b ratio, the compressive strength of specimens with 40% FACs content is higher than that of specimens with 20% FACs content. As can be seen from Figure 14(b), there is no clear and significant correlation between the VMA/b ratio and compressive strength. The effect of VMA/b ratio is more pronounced for the specimens with lower FACs replacement ratios (0% and 20%) while for the specimens with relatively higher FACs content (40% and 60%), the compressive strength is not considerably affected with the VMA/b ratio. Considering the lower limit of compressive strength given in ACI guide for structural lightweight concrete [32], it can be concluded that all the mixtures produced in this study can be used for structural purposes as they have a compressive strength above 30 MPa.

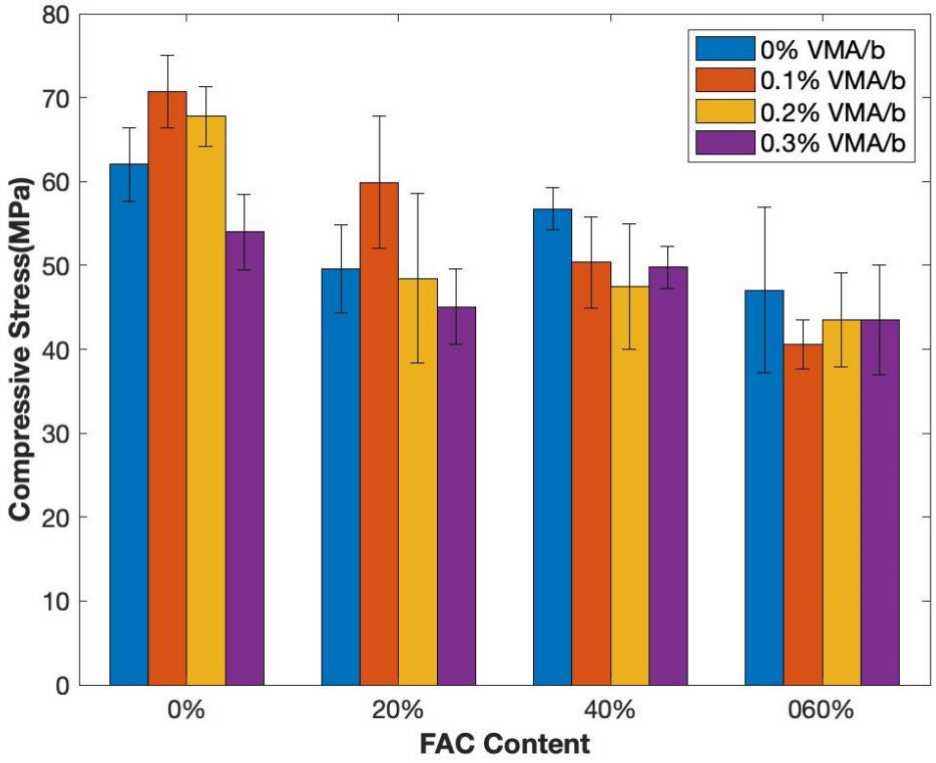

Figure 13. Mean compressive strength of developed mixtures

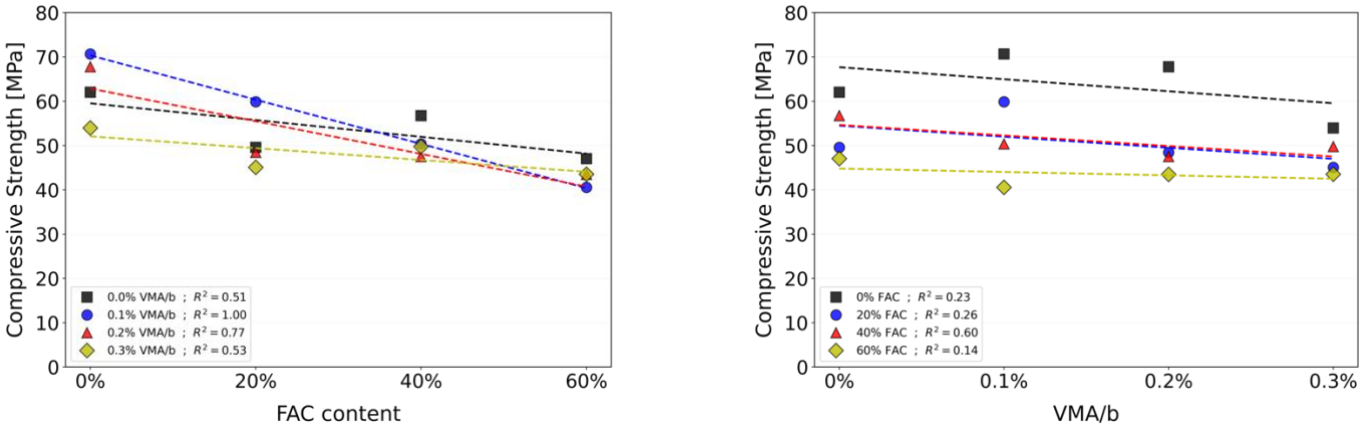

(a) (b)

Figure 14. Variation of compressive strength with (a) FACs content and (b) VMA/b ratio

To further evaluate the effects of FACs on the compressive strength of the developed composites, SEM images of mixtures with a constant VMA/b ratio of 0.1% and varying FACs content is shown in Figure 15 for a low magnification level, while higher magnification SEM images are shown in Figure 16. As shown in Figure 15, the distribution of FACs particle is relatively uniform for all FACs ratios, which shows that a homogeneous mix was achieved during mixing. Note that the spherical nature of FACs alters the packing and usually allows the inclusion of more air. Also, the shell of FACs might have been consumed during pozzolanic reactions, leaving only voids behind. These lead to an increase in porosity and cause a decrease in compressive strength. In addition, the low strength nature of FACs cause decrease in compressive strength. It can be seen from figure 16 that the cracks did not pass through the FACs that has a strong shell and rather propagated through weaker zones around FACs particles. It can be also seen that the FACs acts as nucleation site and help producing more hydration products, which allows to achieve satisfactory compressive strength.

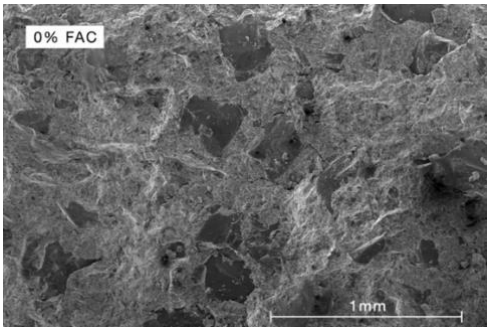

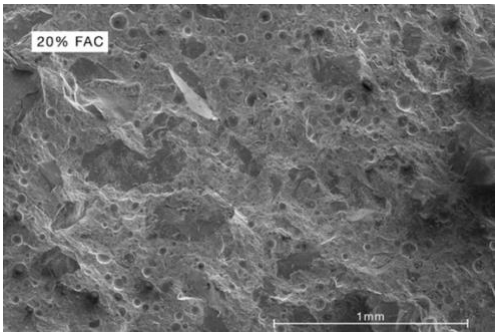

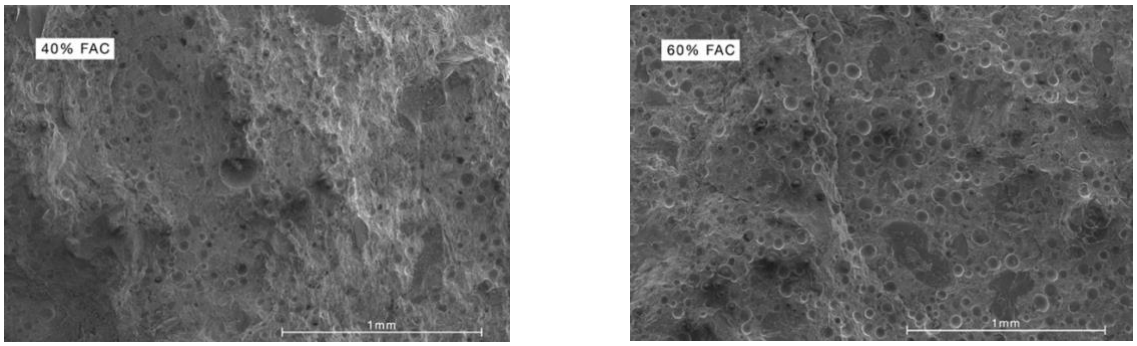

Figure 15. SEM images of mixtures with 0.1% VMA/b ratio and different FACs replacement ratios.

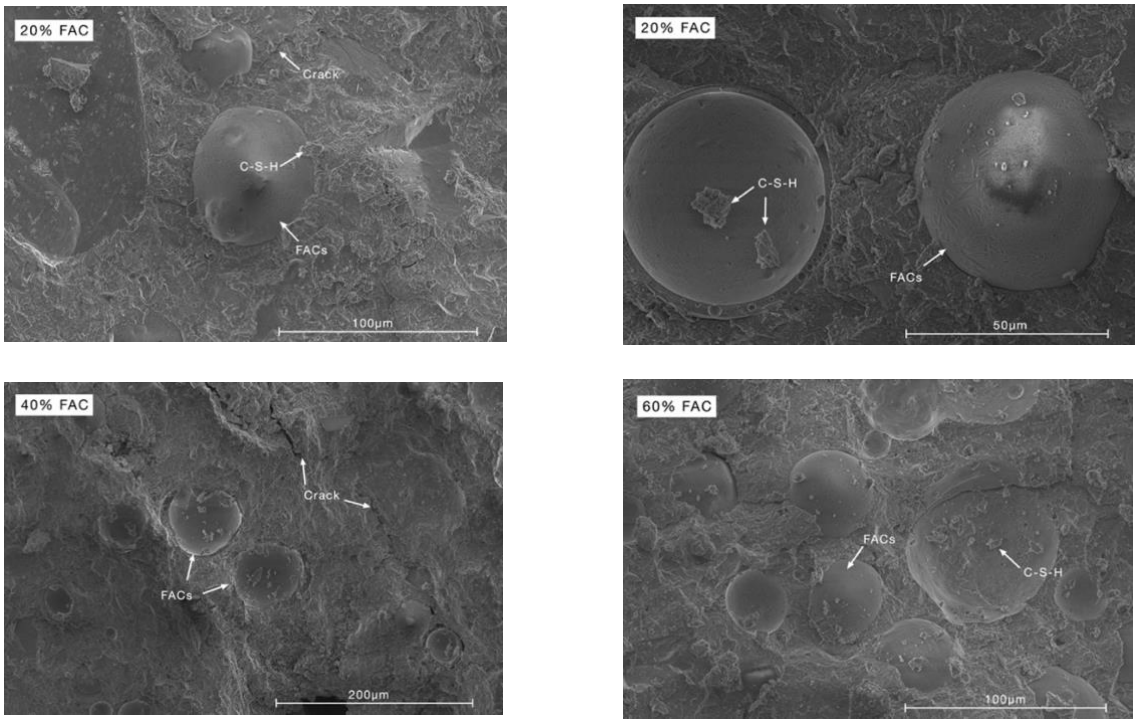

Figure 16. SEM images of mixtures with 0.1% VMA/b ratio and different FACs replacement ratios.

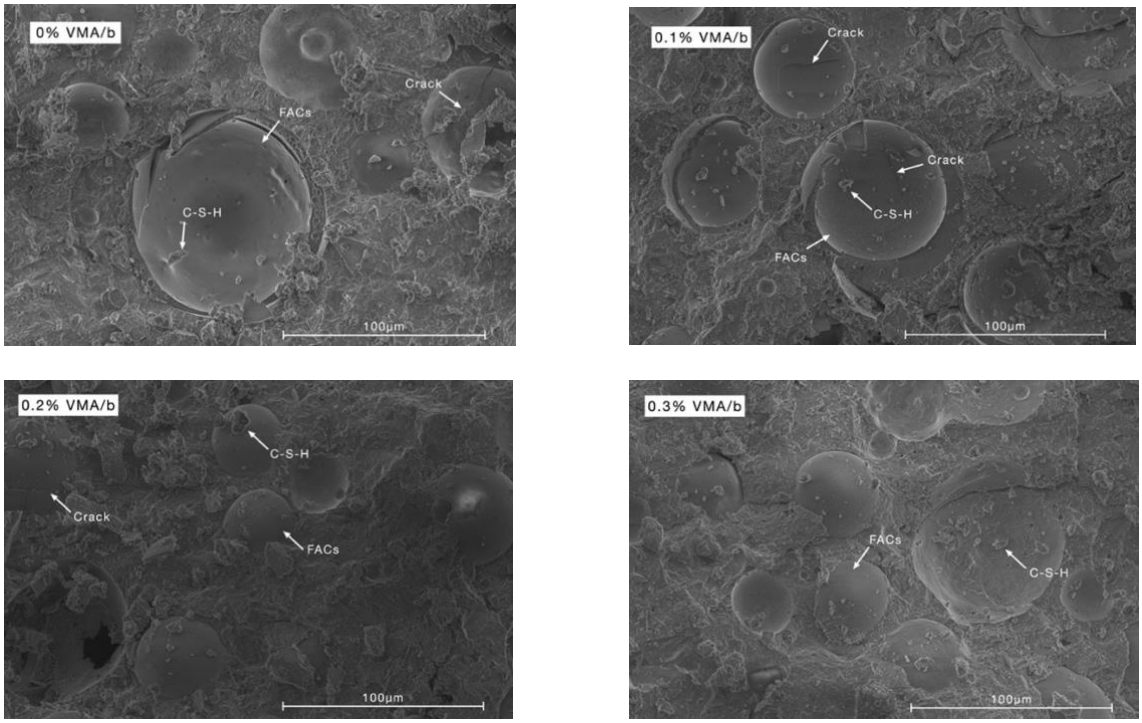

Figure 17. SEM images of mixtures with 60% FACs replacement ratios and different VMA/b ratios.

Figure 17 shows the SEM of mixture with constant FACs replacement ratio at 60% and varying VMA/b ratios with high magnifications. It can be seen that the increase of VMA/b ratio makes no difference on the microstructures of the mixtures which shows that VMA/b ratio has almost no influence on compressive strength.

Figure 18 shows the variation of specific compressive strength of FAC content and VMA/b ratio. Specific compressive strength is the compressive strength of the harden composite divided by its density. This is also known as strength-to-weight ratio. For a certain VMA/b ratio, the relationship between specific compressive strength and FAC replacement fraction is shown in Figure 18(a). For 0.1% and 0.2% VMA/b ratio, specific compressive strength decreases as the FAC replacement fraction increase. However, for 0% and 0.3% VMA/b ratio, there is no good correlation between specific compressive strength and FAC replacement ratio. Nevertheless, we

can see that for these mixtures, the incorporation of FACs at 60% does not lead to a important decrease in specific weight. Moreover, the mixtures with 40% FAC replacement possess a higher strength-to-weight ratio than the control specimen. As shown in Figure 18(b), specific compressive strength reduces slightly with the increase of VMA/b ratio. However, R^2 values from each linear regression fit analysis indicate that correlation between specific compressive strength and VMA/b ratio is not significant. Based on Figure 18, the effects of FAC content and VMA/b ratio are not explicit.

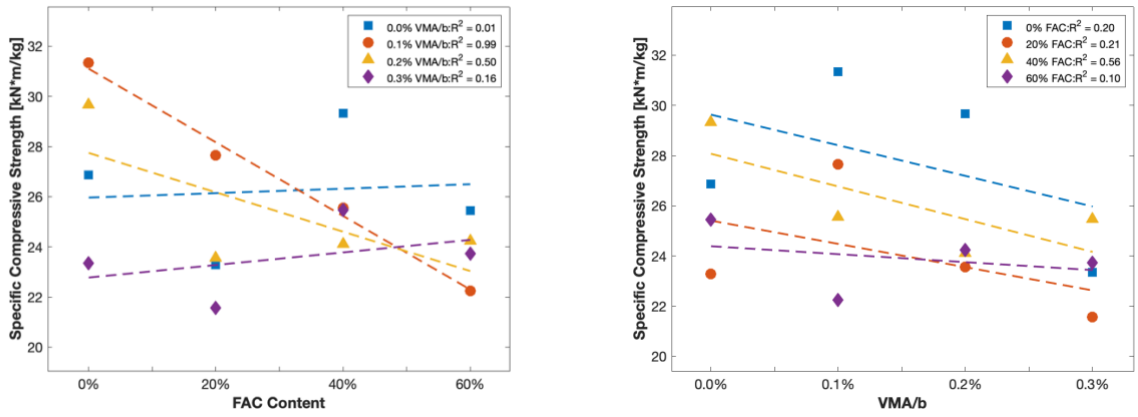

Figure 18. Variation of specific compressive strength of (a) FAC content and (b) VMA/b ratio

4.3 Thermal Conductivity Test Results

Before thermal measurements, the density of the prismatic specimens was measured. Table 8 shows the detailed thermal conductivity test results for all mixtures. Figure 18 shows the density of the developed mixtures with different FACs content. Each data points represent the average density of three specimens for one mix design. Note that for each FACs replacement ratio, there are four density measurement corresponding to the mixtures with different VMA ratio. A reduction in density can clearly be seen from the figure as the FACs content in mixture

increases. The results also indicate that, at a minimum, 40 vol. % of sand needs to be replaced with FACs such that the obtained mixture can be qualified as lightweight concrete according to ACI standards [32].

TABLE 8 Thermal Conductivity of specimens with varying FACs Content and VMA Ratio

Batch	Specimens	FACs Content	VMA Ratio	Density (kg/m^3)	Thermal Conductivity(W/mK)	Average
Mix1	1	0%	0.0%	2313	0.592	0.602
	2	0%	0.0%	2319	0.618	
	3	0%	0.0%	2300	0.594	
Mix2	1	0%	0.1%	2260	0.498	0.538
	2	0%	0.1%	2228	0.484	
	3	0%	0.1%	2279	0.633	
Mix3	1	0%	0.2%	2288	0.501	0.471
	2	0%	0.2%	2291	0.396	
	3	0%	0.2%	2276	0.517	
Mix4	1	0%	0.3%	2303	0.482	0.473
	2	0%	0.3%	2330	0.438	
	3	0%	0.3%	2299	0.500	
Mix5	1	20%	0.0%	2163	0.504	0.532
	2	20%	0.0%	2097	0.548	
	3	20%	0.0%	2128	0.545	
Mix6	1	20%	0.1%	2151	0.441	0.492
	2	20%	0.1%	2142	0.511	
	3	20%	0.1%	2195	0.523	
Mix7	1	20%	0.2%	2048	0.403	0.399
	2	20%	0.2%	2070	0.405	
	3	20%	0.2%	2058	0.389	
Mix8	1	20%	0.3%	2096	0.443	0.393
	2	20%	0.3%	2083	0.405	
	3	20%	0.3%	2088	0.331	
Mix9	1	40%	0.0%	1914	0.456	0.428
	2	40%	0.0%	1921	0.379	
	3	40%	0.0%	1969	0.448	
Mix10	1	40%	0.1%	1932	0.327	0.397
	2	40%	0.1%	1986	0.426	
	3	40%	0.1%	1993	0.437	
Mix11	1	40%	0.2%	1950	0.422	0.389
	2	40%	0.2%	1964	0.331	

	3	40%	0.2%	1990	0.413	
Mix12	1	40%	0.3%	1955	0.394	0.354
	2	40%	0.3%	1946	0.345	
	3	40%	0.3%	1960	0.322	
Mix13	1	60%	0.0%	1851	0.378	0.399
	2	60%	0.0%	1855	0.405	
	3	60%	0.0%	1843	0.415	
Mix14	1	60%	0.1%	1814	0.387	0.388
	2	60%	0.1%	1826	0.363	
	3	60%	0.1%	1830	0.415	
Mix15	1	60%	0.2%	1808	0.310	0.338
	2	60%	0.2%	1767	0.315	
	3	60%	0.2%	1812	0.389	
Mix16	1	60%	0.3%	1833	0.345	0.369
	2	60%	0.3%	1821	0.356	
	3	60%	0.3%	1850	0.406	

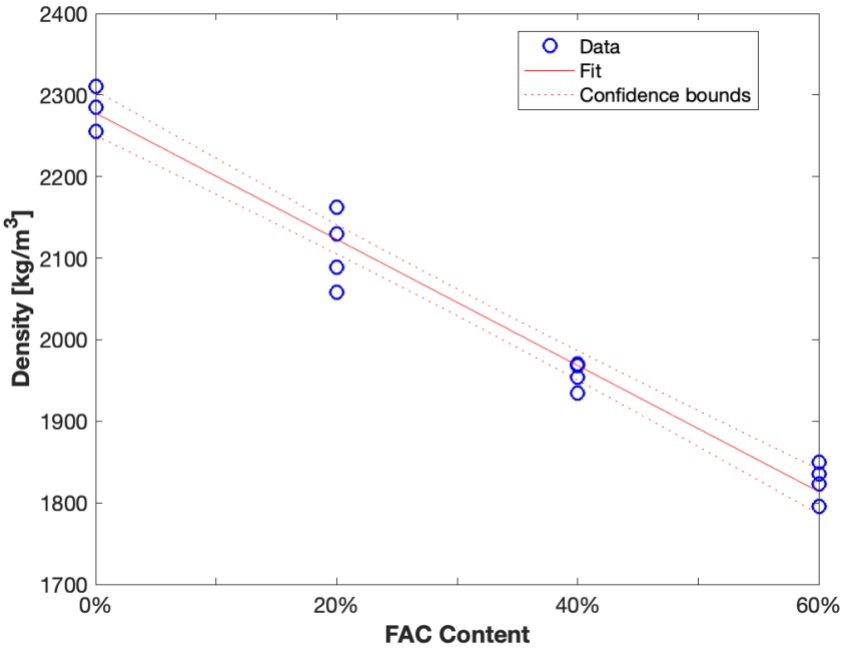

Figure 19. Variation of density with FAC replacement ratio for all mixtures

Figure 19 shows the relationship between the measured thermal conductivity and density of the tested specimens, while Figure 20 illustrates the variation of thermal conductivity with

FACs. It can be seen from Figure 19 that thermal conductivity values of the cementitious composites correlate with the density of the specimens. As expected, the specimens with lower density have also lower thermal conductivity, implying better thermal insulation properties for the specimens with FACs. In addition, most of the data point are inside the confidence bounds, which indicates a good correlation between thermal conductivity and density. Similar but inverse correlation exists between the thermal conductivity and FAC content, i.e. increasing the FAC content decreases the thermal conductivity. Due to the hollow structure of FACs, increasing the FAC content in cementitious composites leads to the increasing of porosity of the mixture. In addition, with FACs' air-filled nature, adding FAC content essentially equals adding air inside the mixture. Since air is less thermally conductive than concrete mortar, the thermal conductivity of the harden composite decreases with more FAC content.

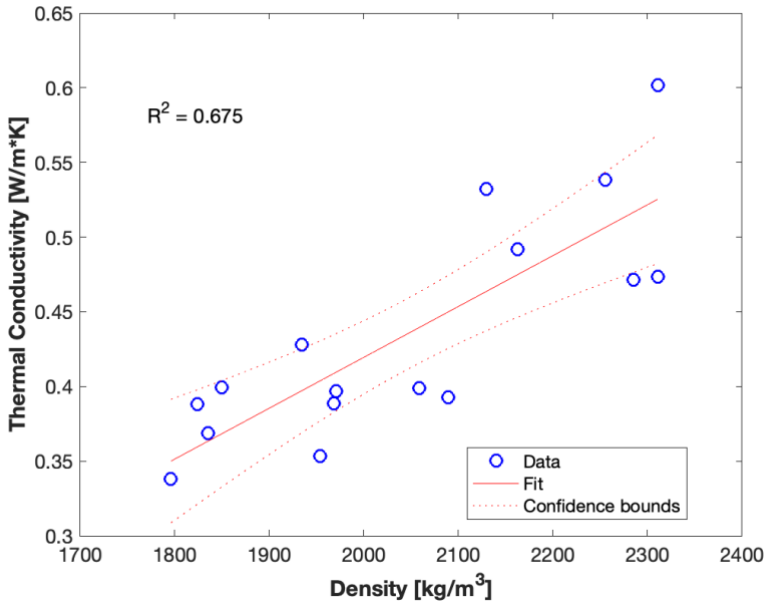

Figure 20. Variation of thermal conductivity with density for all mixtures

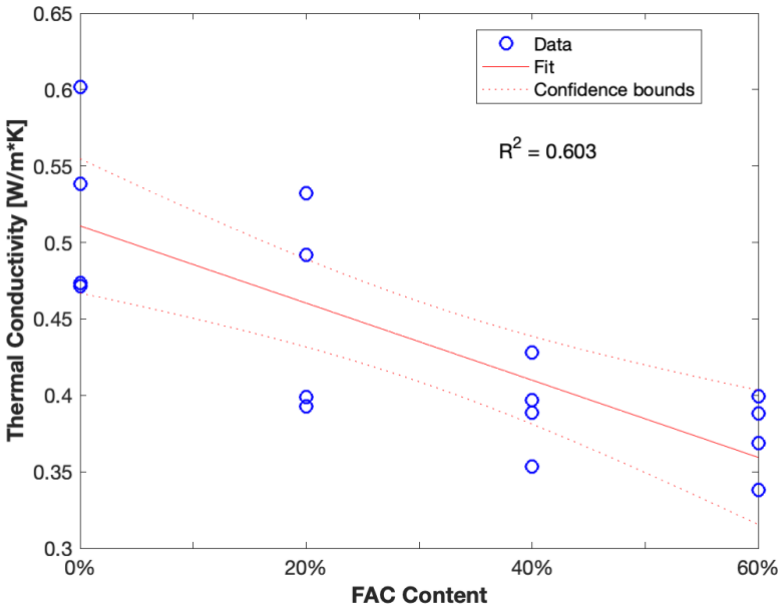

Figure 21. Variation of thermal conductivity with FAC replacement ratio for all mixtures

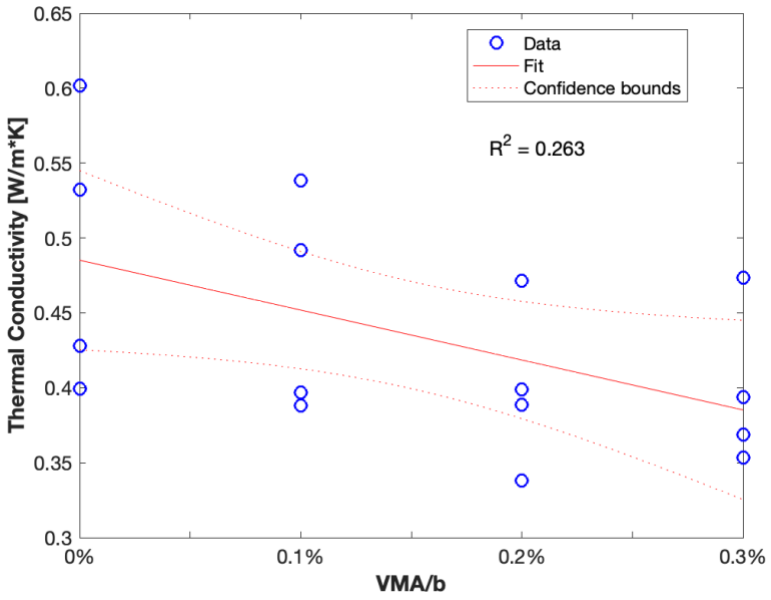

Figure 22. Variation of thermal conductivity with VMA/b ratio for all mixtures

Figure 21 shows the relationship between measured thermal conductivity and the VMA/b ratio of all the specimens. It is difficult to conclude based on Figure 21 that thermal conductivity correlates with VMA/b ratio. Linear regression analysis ($R^2 = 0.263$) also indicates that VMA/b ratio has little influence on the thermal conductivity of the harden composites. In order to further assess the effects of FAC content and VMA on the thermal conductivity of mixtures, Figure 22 shows the average thermal conductivity of mixtures with different FACs content. The bar plots are grouped based on the VMA/b ratios. It can be seen that increasing the FACs content or VMA/b ratio decreases the thermal conductivity of the specimens. For the specimens with 60% FACs, the thermal conductivity of the tested specimens ranged from 0.399 to 0.338 W/m K.

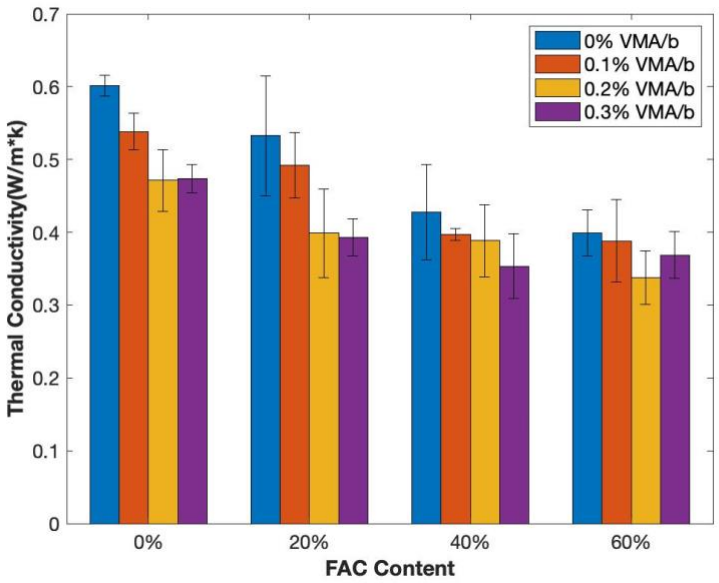

Figure 23. Mean thermal conductivity of developed mixtures

Figure 23(a) shows the variation of thermal conductivity with FACs content for each VMA/b ratio, while the variation of thermal conductivity with VMA/b ratio for each FACs content is illustrated in Figure 23(b). Although a decreasing trend in thermal conductivity with increasing VMA/b ratio or FACs content is clear, the rate of this decrease is generally higher

with the FACs content compared to VMA/b ratio. It can also be seen that increasing FACs content at the specimens with lower VMA/b ratio (0% or 0.1%) leads higher decreases in thermal conductivity compared to the specimens with a higher VMA/b ratio (0.2% and 0.3%). Similarly, as can be seen in Figure 23(b), there is a high correlation with an increase in VMA/b ratio and a decrease in thermal conductivity for specimens with low FACs content (0% or 20%). On the other hand, the effect of VMA/b ratio on thermal conductivity of the specimens with high FACs content (40% or 60%) is considerably lower.

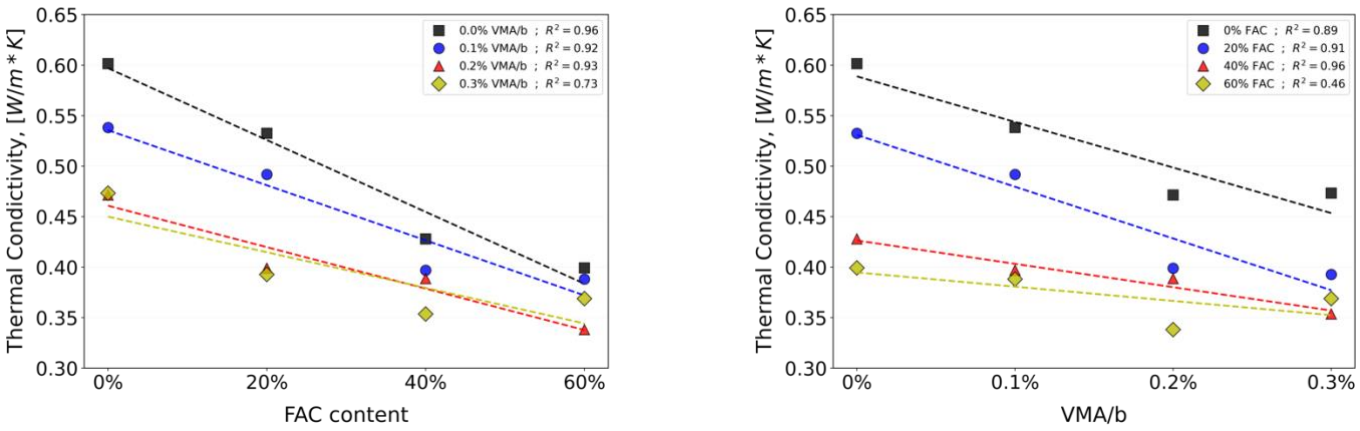

(a) (b)

Figure 24. Variation of thermal conductivity with (a) FACs content and (b) VMA/b ratio

4.4 Buildability Test Results

Figure 24 shows the scatter plot for static yield stress versus thermal conductivity of all tested mixtures. As the mixture with 0.3% VMA/b ratio and 60% FACs ratio had the highest yield stress, one of the lowest thermal conductivity as well as sufficient compressive strength for structural applications, this particular mixture was selected for printability study. As discussed earlier, to classify the mixture as buildable for the target application described in earlier section, at least 20 layers need to be printed with rectangular cross-section nozzle. This target number of layers were achieved as shown in figure 25(a) without any collapse. Printed structure was cut

vertically in order to visualize the connections of the layers as well as the dimensions of each layer as shown in Figure 23(b). No clear interface was observed between the layers which suggests that 60 s time gap between the layers can be sufficient for a proper connection of the layers.

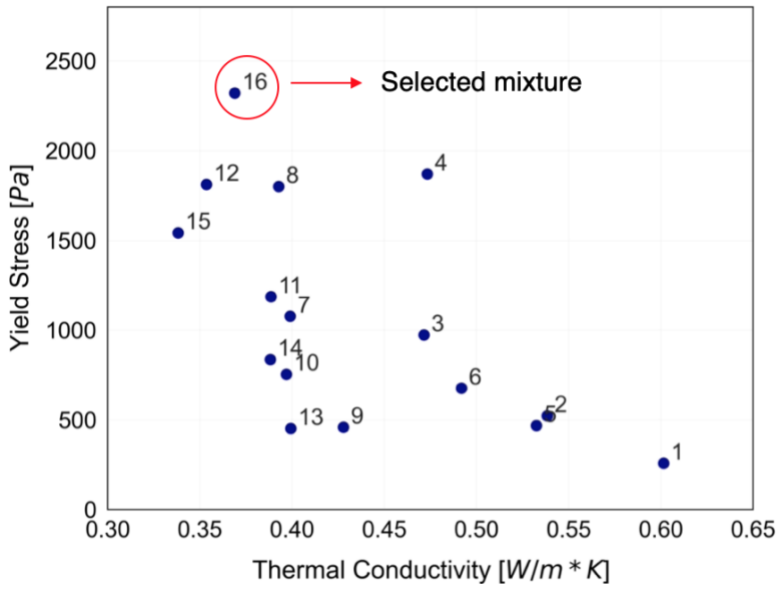

Figure 25. Static yield stress versus thermal conductivity

For the nozzle with rectangular cross-section, the theoretical breadth (B_{theo}) and height (h_{theo}) of each layer are 30 mm and 15 mm, respectively, and with the aimed 20 layers, the theoretical total height (H_{theo}) was calculated as 300 mm. However, after extrusion of each layer, the breadth and height of each layer were about 35 mm and 14 mm for each layer. Figure 26 shows the dimensions of each layer after printing and the variation of the total height of the structure with the number of printed layers. Solid lines in the Figure 26(a) represents the theoretical dimensions of the layers while the dotted lines with triangle markers represent the experimental dimensions. It can be seen that the height of each layer except the first and second

layers remained almost unchanged. Note that a relatively short time gap (60 s) between layers was selected in this study. A somewhat increase in the time gap between printed layer may further improve shape stability of the printed layers, especially first two layers.

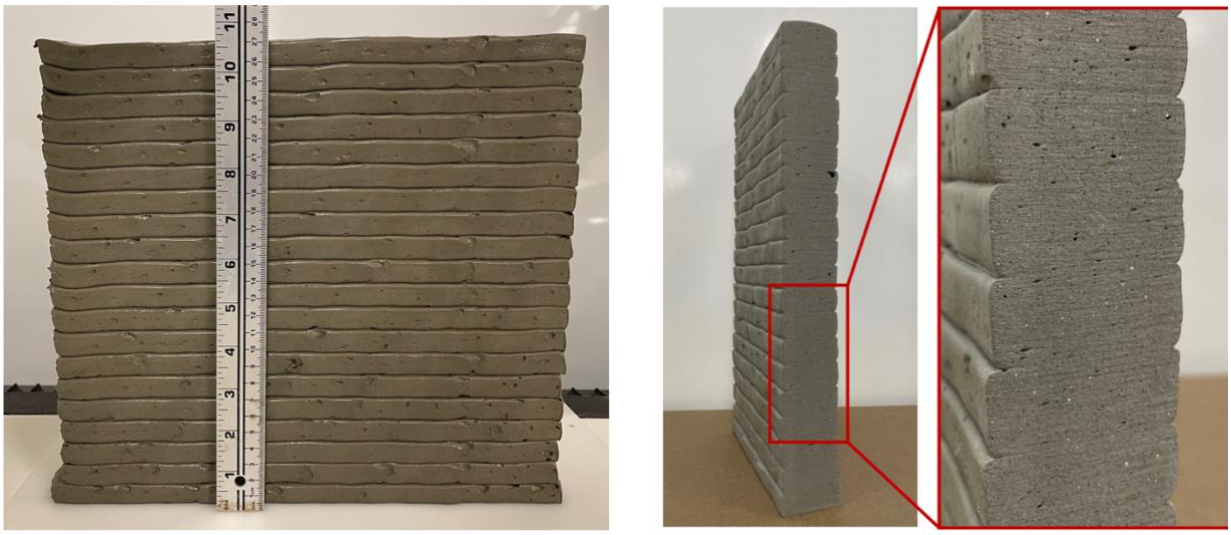

(a) (b)

Figure 26. FACs-based cementitious composites layers printed with a rectangular nozzle

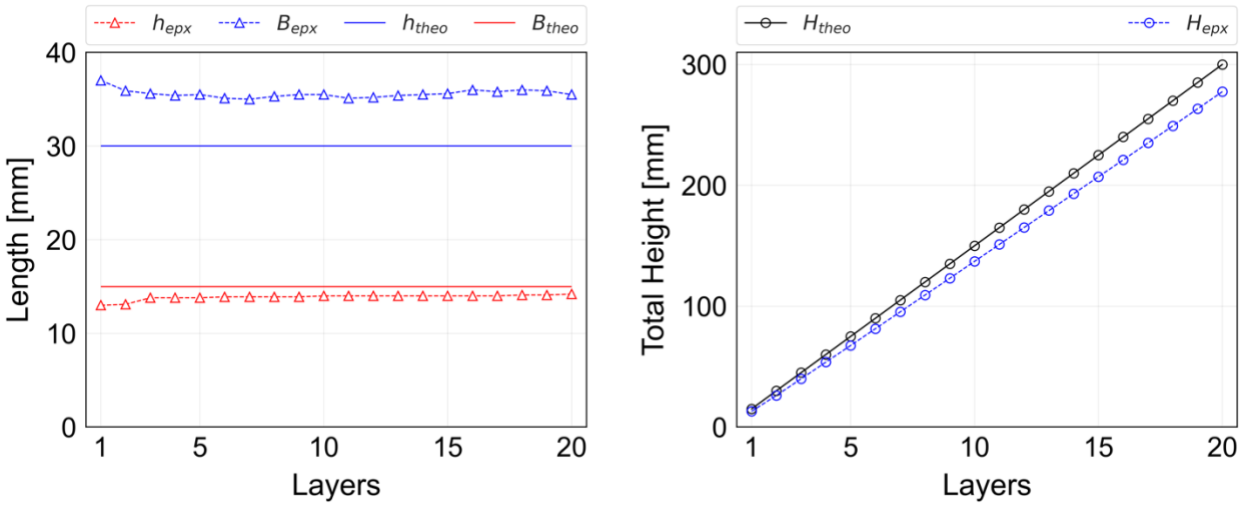

(a) (b)

Figure 27. (a) Theoretical and experimental dimensions of each layer, and (b) total height of the structure with number of layers

Buildability of the same mixture was also studied with a circular nozzle via vertical extrusion. Note that a minimum of 23 layers must be printed for successful completion of buildability test for this case according to the theoretical calculations. During this buildability tests, the printing of the layers was continued until the use of all prepared mixture. In this case, the maximum number of layers achieved before collapse was recorded as 31 layers as shown in Figure 27. As the printing continued until collapse, the thickness of each layer could not be measured and recorded in this case. Overall, the developed mixture showed satisfactory shape stability and buildability performance during the direct buildability testing with two different nozzles.

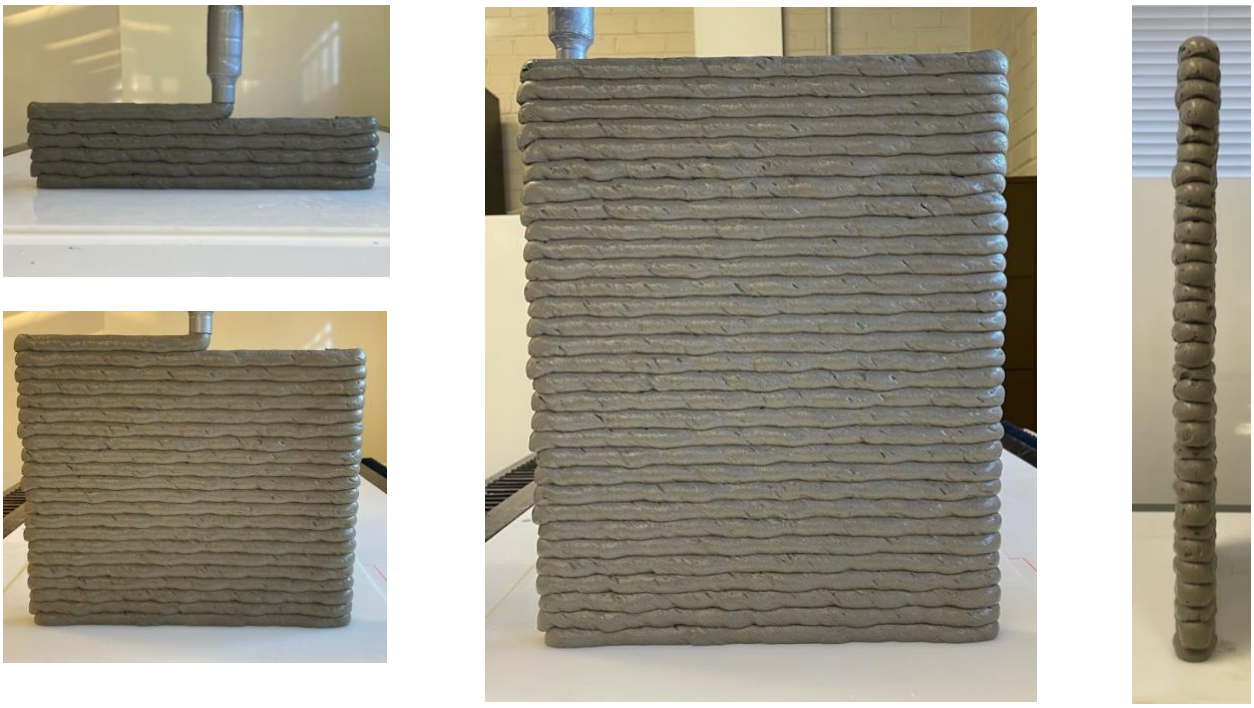

Figure 28. FACs-based cementitious composites layers printed with a circular nozzle

5. CONCLUSIONS

This thesis investigated the development of lightweight cementitious composites with fly ash cenospheres for 3D concrete printing applications. First, the effects of FACs content and viscosity modifying agent on rheological properties of FACs-based cementitious composites were studied. The effect of FACs content and VMA on the mechanical and thermal properties of FACs-based cementitious composite were also investigated. The percentage replacement of sand with FAC content varies from 0% to 60%. The VMA usage in the mixture varies from 0% to 0.3%.

The findings of this study can be summarized as follows:

- FACs do not have a considerable effect on the yield stress of the developed mixtures, while the yield stress can be considerably increased using 0.2% or 0.3% VMA by weight of binders. Yield stress and viscosity are positively proportional related to the VMA content.
- Densities of hardened cementitious composites decrease linearly with the increase of FACs content. The densities of composites ranged from 2310.9 kg/m^3 to 1795.9 kg/m^3. Based on the results, only mixtures with 40% or higher FACs content can be qualified as lightweight concrete. The replacement of FACs with sand up to 60% decreased the density of cementitious mixture by 22%.
- The compressive strength of the developed composite ranged from 70.7 MPa to 40.6 MPa, indicating high compressive strength for even the mixtures with highest FACs replacement ratio. Due to the low strength nature of FAC, compressive strength of hardened composites reduces as the replacement of sand by FAC content increases.

- Thermal conductivity results showed that the addition of FACs content can considerably improve the thermal insulation properties of the developed cementitious composites. In particular, the thermal conductivity of the FACs-based composites with 60% FACs replacement ratio was as low as 0.338 W/m K. In addition, a good correlation was observed between the density of the material and thermal conductivity.
- A printability test simulating a residential building wall was conducted with FACs-based composites with 60% FACs replacement ratio. Printing with a horizontal nozzle and a circular nozzle, 23 layers were selected to be the minimum number of layers for determining the buildability of FACs-based composites. In the end, composites were able to be printed to the desire number of layers with both nozzles. A maximum of 31 layers was printed before collapse.

Overall, the results indicate that FACs can be used to develop lightweight cementitious composites with good thermal and mechanical properties for additive construction. VMA can be utilized to enhance the buildability of the FACs-based composites by improving rheological performance of the material.

Future studies can explore in the following areas:

- The possible difference in the mechanical and thermal performance of the composites when the specimens are casted with 3D concrete printing other than traditional casting method. Since the specimens need to cut into required sizes for compressive strength and thermal conductivity tests after 3D printing, further studies can be conducted to determine if the different casting method can cause difference in performance for both mechanical and thermal properties.

- During this thesis study, only one size of FAC was utilized. Thus, the effects on rheological, mechanical and thermal performance of the composite are unknown and should be studied.
- The effect of FACs and VMA content on the shrinkage of the harden concrete composites is another area can be explored. VMA fix some water molecules to the periphery of chain [26]. Thus, with increase of VMA content, the water molecules available to react with cement reduce slightly. Therefore, the shrinkage of harden composite reduces resulting from less Portland cement hydration process. FAC has relatively high-water absorption rate. Similar to increase VMA content in concrete composite, increase FACs content can cause less cement hydration resulting a reduced shrinkage.
- Because of the spherical shape of FAC, there is potential weakening of the interlayer bond strength between printed layers. The interlayer bond strength between printed layers of 3D printable cementitious composite with FACs should be studied.

References

1. Wang, X., Chen, D., & Ren, Z. (2010). Assessment of climate change impact on residential building heating and cooling energy requirement in Australia. *Building and Environment*, *45*(7), 1663-1682.
2. Tushar, Q., Bhuiyan, M., Sandanayake, M., & Zhang, G. (2019). Optimizing the energy consumption in a residential building at different climate zones: Towards sustainable decision making. *Journal of Cleaner Production*, 233, 634-649.
3. Hester, J., Gregory, J., Ulm, F. J., & Kirchain, R. (2018). Building design-space exploration through quasi-optimization of life cycle impacts and costs. *Building and Environment*, *144*, 34-44.
4. Z. Huang, F. Wang, Y. Zhou, L. Sui, P. Krishnan, J.Y.R. Liew. "A novel, multifunctional, floatable, lightweight cement composite: development and properties." *Materials* 11, no. 10 (2018): 2043.
5. *2015 Residential Energy Consumption Survey,* U.S. Energy Information Administration (Washington, DC, last updated August 4, 2020)
6. A. Dixit, S. D. Pang, S. Kang, J. Moon. "Lightweight structural cement composites with expanded polystyrene (EPS) for enhanced thermal insulation." *Cement and Concrete Composites* 102 (2019): 185-197.
7. H. Shoukry, M. F. Kotkata, S. A. Abo-EL-Enein, M. S. Morsy, and S. S. Shebl. "Thermo-physical properties of nanostructured lightweight fiber reinforced cementitious composites." *Construction and Building Materials* 102 (2016): 167-174.

8. D. Kramar, Derek, V. Bindiganavile. "Mechanical properties and size effects in lightweight mortars containing expanded perlite aggregate." *Materials and Structures* 44, no.4, (2011): 735-748.
9. J. Zhang, J. Wang, S. Dong, X. Yu, and B. Han, "A review of the current progress and application of 3D printed concrete", *Composites Part A: Applied Science and Manufacturing* 125, (2019): 105533.
10. Bing Lu, Ye Qian, Mingyang Li, Yiwei Weng, Kah Fai Leong, Ming Jen Tan, Shunzhi Qian, "Designing spray-based 3D printable cementitious materials with fly ash cenoshpere and air entraining agent", *Construction and Building Materials* 211, (2019): 1073-1084.
11. X. Huang, R. Ranade, Q. Zhang, W. Ni, V.C. Li. "Mechanical and thermal properties of green lightweight engineered cementitious composites." *Construction and Building Materials* 48 (2013): 954-960.
12. Hongyu Zhou, Adam L. Brooks, "Thermal and mechanical properties of structural lightweight concrete containing lightweight aggregates and fly-ash cenoshperes", *Construction and Building Materials* 198, (2019): 512-526.
13. H.P. Satpathy, S.K. Patel, A.N. Nayak, "Development of sustainable lightweight concrete using fly ash cenoshpere and sintered fly ash aggregate", *Construction and Building Materials* 202, (2019): 636-655.
14. Sudeep K. Patel, Hara P. Satpathy, Amar N. Nayak, Chitta R. Mohanty, "Utiliztion of Fly Ash Cenoshpere for Production of Sustiainable Lightweight Concrete", *Journal of The Institution of Engineers (India): Series A* 101(1), (2020): 179-194

15. Asad Hanif, Pavithra Parthasarathy, Hongyan Ma, Tianyuan Fan, Zongjin Li, “Properties improvement of fly ash cenosphere modified cement pastes using nano silica”, *Cement and Concrete Composites* 81, (2017): 35-48
16. Vanessa Rheinheimer, Yunpeng Wu, Tao Wu, Kemal Celik, Junyan Wang, Laura De Lorenzis, Peter Wriggers, Min-Hong Zhang, Paulo J.M. Monteiro, “Multi-scale study of high-strength low-thermal-conductivity cement composites containing cenospheres”, *Cement and Concrete Composites* 80, (2017): 91-103
17. Yu Zhang, Yunsheng Zhang, Wei She, Lin Yang, Guojian Liu, Yonggan Yang, “Rheological and harden properties of the high-thixotropy 3D printing concrete”, *Construction and Building Materials* 201, (2019): 278-285.
18. Yiwei Weng, Mingyang Li, Ming Jen Tan, Shunzhi Qian, “Design 3D printing cementitious materials via Fuller Thompson theory and Marson-Percy model”, *Construction and Building Materials* 163, (2018): 600-610
19. Devid Falliano, Dario De Domenico, Giuseppe Ricciardi, Ernesto Gugliandolo, “3D-printable lightweight foamed concrete and comparison with classical foamed concrete in terms of fresh state properties and mechanical strength”, *Construction and Building Materials* 254, (2020): 119-271.
20. Guan Heng Andrew Ting, Yi Wei Daniel Tay, Ye Qian, Ming Jen Tan, “Utilization of recycled glass for 3D concrete printing: rheological and mechanical properties”, *Journal of Material Cycles and Waste Management* 21, (2019): 994-1003
21. Karla Cuevas, Mehdi Chougan, Falk Martin, Seyed Hamidreza Ghaffar, Dietmar Stephan, Pawel Skikora, “3D printable lightweight cementitious composites with incorporated waste

glass aggregates and expanded microspheres – Rheological, thermal and mechanical properties", *Journal of Building Engineering* 44, (2021): 102718

22. Thomas G. Mezger, "Applied Rheology with Joe Flow on Rheology Road", Anton Paar Gmbh, 4th edition (May 2017)
23. *Standard Test Method for Steady-State Thermal Transmission Properties by Means of the Heat Flow Meter Apparatus,* ASTM C518-17 (West Conshohocken, PA: ASTM International, approved May 1, 2017).
24. *Operating Manual HFM 446 Lambda – Series*, Netzsch, version 1.5, October 2018
25. *Standard Specification for Portland Cement,* ASTM C150/C150M-20 (West Conshohocken, PA: ASTM International, approved April 1, 2020).
26. Mohammed Sonebi, "Rheological properties of grouts with viscosity modifying agents as diutan gum and welan gum incorporating pulverized fly ash", Cement and Concrete Research 36 (2006): 1609-1618.
27. *Standard Test Method for Compressive Strength of Hydraulic Cement Mortars (Using 2-in. or [50 mm] Cube Specimens),* ASTM C109/C109M-20b (West Conshohocken, PA: ASTM International, approved April 1, 2020).
28. V. N. Nerella, K. M. Krause, and V. Mechtcherine, "Direct printing test for buildability of 3D-printable concrete considering economic viability," *Automation in Construction* 109 (2020): 102986.
29. M. S. Huffman, J. R. Baty, "Guide to Residential Concrete Construction", American Concrete Institute, ACI 332.1R-06

30. Y. W. D. Tay, G. H. A. Ting, Y. Qian, B. Panda, L. He, and M. J. Tan, “Time gap effect on bond strength of 3D-printed concrete.” *Virtual and Physical Prototyping* 14, no. 1 (2019): 104-113.
31. Panda, S. C. Paul, N. A. N. Mohamed, Y. W. D. Tay, and M. J. Tan. “Measurement of tensile bond strength of 3D printed geopolymer mortar.” *Measurement* 113 (2018): 108-116.
32. H. C. Robinson, A. B. Spamer, “Guide for Structural Lightweight Aggregate Concrete”, American Concrete Institute, ACI 213R-87